Washington University School of Medicine
Digital Commons@Becker

Open Access Publications

2014

Monitoring of biodistribution and persistence of conditionally replicative adenovirus in a murine model of ovarian cancer using capsid-incorporated mCherry and expression of human somatostatin receptor subtype 2 gene

Igor P. Dmitriev
Washington University School of Medicine in St. Louis

Elena A. Kashentseva
Washington University School of Medicine in St. Louis

Walter J. Akers
Washington University School of Medicine in St. Louis

Samuel Achilefu
Washington University School of Medicine in St. Louis

David T. Curiel
Washington University School of Medicine in St. Louis

Recommended Citation

Dmitriev, Igor P.; Kashentseva, Elena A.; Akers, Walter J.; Achilefu, Samuel; Curiel, David T.; and et al ,"Monitoring of biodistribution and persistence of conditionally replicative adenovirus in a murine model of ovarian cancer using capsid-incorporated mCherry and expression of human somatostatin receptor subtype 2 gene." Molecular Imaging.13,8. 1-19. (2014).
http://digitalcommons.wustl.edu/open_access_pubs/4806

See next page for additional authors

Authors

Igor P. Dmitriev, Elena A. Kashentseva, Walter J. Akers, Samuel Achilefu, David T. Curiel, and et al

Monitoring of Biodistribution and Persistence of Conditionally Replicative Adenovirus in a Murine Model of Ovarian Cancer Using Capsid-Incorporated mCherry and Expression of Human Somatostatin Receptor Subtype 2 Gene

Igor P. Dmitriev, Elena A. Kashentseva, Kenneth H. Kim, Qiana L. Matthews, Stephanie S. Krieger, Jesse J. Parry, Kim N. Nguyen, Walter J. Akers, Samuel Achilefu, Buck E. Rogers, Ronald D. Alvarez, and David T. Curiel

Abstract

A significant limiting factor to the human clinical application of conditionally replicative adenovirus (CRAd)-based virotherapy is the inability to noninvasively monitor these agents and their potential persistence. To address this issue, we proposed a novel imaging approach that combines transient expression of the human somatostatin receptor (SSTR) subtype 2 reporter gene with genetic labeling of the viral capsid with mCherry fluorescent protein. To test this dual modality system, we constructed the Ad5/3Δ24pIXcherry/SSTR CRAd and validated its capacity to generate fluorescent and nuclear signals in vitro and following intratumoral injection. Analysis of ^{64}Cu-CB-TE2A-Y3-TATE biodistribution in mice revealed reduced uptake in tumors injected with the imaging CRAd relative to the replication–incompetent, Ad-expressing SSTR2 but significantly greater uptake compared to the negative CRAd control. Optical imaging demonstrated relative correlation of fluorescent signal with virus replication as determined by viral genome quantification in tumors. Positron emission tomography/computed tomography studies demonstrated that we can visualize radioactive uptake in tumors injected with imaging CRAd and the trend for greater uptake by standardized uptake value analysis compared to control CRAd. In the aggregate, the plasticity of our dual imaging approach should provide the technical basis for monitoring CRAd biodistribution and persistence in preclinical studies while offering potential utility for a range of clinical applications.

I N THE PAST TWO DECADES, gene therapy has been developed as a promising approach to combat a variety of diseases. Over this time period, more than 1,700 clinical gene therapy trials were conducted, with 65% addressing cancer.[1] Adenoviral vectors have been used in 24% of clinical trials, followed by retroviral vectors (21%) and naked/plasmid DNA (19%). Thus far, gene transfer efficiency has been evaluated by obtaining tissue biopsies at predetermined times posttreatment. This method of determining gene transfer efficiency is undesirable due to its invasiveness and its inability to generate a global picture of gene transfer because it is limited to the small piece of tissue(s) examined. It is evident that gene therapy trials would benefit from the ability to determine the location of gene delivery vectors and evaluate the magnitude of expression of the delivered genes over time.

Human adenovirus[2] (Ad) has been used extensively to develop replication-deficient gene delivery vectors and conditionally replicative adenovirus (CRAd) agents for cancer treatment. We previously evaluated several gene therapy strategies including oncolytic CRAd virotherapy for ovarian cancer.[3,4] This approach takes advantage of the propensity of human Ad to infect and replicate in epithelial

From the Division of Cancer Biology, Department of Radiation Oncology, School of Medicine, and Mallinckrodt Institute of Radiology, School of Medicine, Washington University, St. Louis, MO; Division of Gynecologic Oncology, The University of North Carolina, Chapel Hill, NC; and Divisions of Infectious Diseases and Gynecologic Oncology, The University of Alabama at Birmingham, Birmingham, AL.

Address reprint requests to: Igor P. Dmitriev, PhD, Department of Radiation Oncology, Washington University School of Medicine, 4511 Forest Park Avenue, Suite 411, St. Louis, MO 63108; e-mail: idmitriev@radonc.

DECKER℞

cells, the origin of most human cancers, while promoting cell lysis to facilitate release of viral progeny.[2] These features have been exploited by a number of strategies aimed at creating oncolytic CRAd vectors with increased selectivity for cancer cells.[5] We showed that the clinical utility of CRAds derived from adenovirus serotype 5 (Ad5) for oncolytic treatment of ovarian carcinoma is hampered by inefficient infection of ovarian cancer cells due to the paucity of coxsackievirus group B and Ad receptor (CAR), the primary Ad5 receptor.[6–8] To confer CAR-independent virus tropism, we used genetic incorporation of RGD-4C targeting peptide into Ad5 fiber knob domain[9] or the knob replacement for its counterpart from Ad serotype 3[10] that recognizes an alternative receptor, desmoglein 2,[11] which appears to be more abundantly expressed in ovarian cancer cells.[12,13] These capsid modifications were employed to alter tropism of CRAd Delta-24,[14] which contains a 24-basepair deletion in the E1A conserved region 2, allowing selective replication within Rb-p16-deficient tumor cells,[15] a defect observed in most ovarian cancer cells.[16,17] We showed that Delta24-RGD and Ad5/3Δ24 CRAd derivatives exhibit superior antitumor efficacy in murine models of carcinoma of the ovary.[18–20] Both of these CRAds have been translated into phase I human clinical trials. These studies documented the safety of these agents.[21,22] Although these studies provided useful surrogate end points suggesting therapeutic activity, the acquisition of additional data that would have guided the rational development of improved CRAd agents was limited by current vector design.

The ability to monitor virus biodistribution and persistence could provide critical data about the tumor-targeting efficacy of CRAd vectors and their safety in the human context. On this basis, we considered strategies to acquire these useful end points via imaging analysis to allow the derivation of the maximal scientific value from endeavored clinical trials. The major molecular imaging modalities that are readily translatable to the clinic are magnetic resonance imaging and nuclear imaging, including positron-emission tomography (PET), gamma ray, or single-photon emission computed tomography (SPECT).[23] We previously demonstrated that the human somatostatin (SST) receptor subtype 2 (SSTR2) can be used to assess the efficacy of in vivo gene transfer in a clinical trial using a replication-incompetent Ad vector by employing a Food and Drug Administration–approved SST analogue reporter probes for SPECT imaging.[24] However, SSTR2 has not been evaluated as an imaging reporter gene in the CRAd context. As an alternative to conventional vector detection techniques, we developed a highly novel specific genetic labeling system whereby an Ad vector incorporates a fusion between

capsid protein IX and imaging reporter.[25–28] We also demonstrated that genetic capsid labeling with fluorescent proteins[25] allows direct real-time analysis of in situ virus localization using noninvasive optical imaging[29,30] in pre-clinical cancer models, thus providing a promising approach for the dynamic assessment of oncolytic CRAd function in vivo. On the basis of these considerations, we sought to design a CRAd agent that also embodies the "double imaging" capacity we defined in our foregoing studies. To this end, we engineered the Ad5/3Δ24 CRAd to display mCherry fluorescent protein at the pIX locale while expressing the SSTR2 gene in the E3 region (Figure 1). We validated the capacity of the constructed Ad5/3Δ24pIXcherry/SSTR CRAd to generate fluorescent and nuclear signals in a murine model of subcutaneous ovarian tumor xenografts compared to replication-deficient Ad5/3-SSTRpIXcherry vector and Ad5/3Δ24pIXcherry CRAd, thus demonstrating the potential utility of our double imaging approach for preclinical and human clinical employ. This novel linkage of imaging modalities provides the potential to dramatically enhance
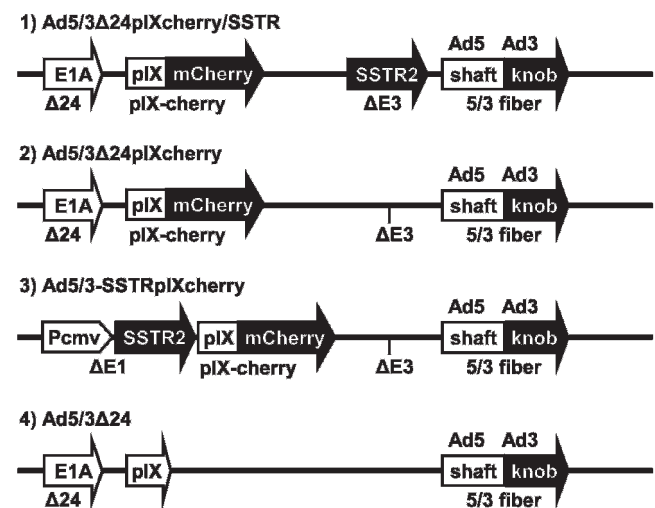
Figure 1. Graphical representation of Ad vectors used in the study. The genomes of Ad5/3Δ24pIXcherry/SSTR (1), Ad5/3Δ24pIXcherry (2), and Ad5/3Δ24 (4) CRAd vectors and replication-incompetent Ad5/3-SSTRpIXcherry (3) vector are shown. The CRAd vectors (1, 2, and 4) have a deletion of 24 nucleotides (Δ24) in the early E1A gene (*E1A*) to allow selective replication in tumor cells with an pRb mutation. The protein IX (*pIX*) gene is modified in all three vectors to encode the C-terminal mCherry fluorescent protein (pIX-cherry). All three vectors encode a chimeric fiber protein (5/3 fiber) containing tail and shaft regions of Ad5 fiber fused with knob domain of Ad3. Ad5/3Δ24pIXcherry/SSTR vector contains gene encoding human SSTR2, which is incorporated in place of the deleted E3 region (ΔE3), under transcriptional control of Ad major late promoter. Ad5/3-SSTRpIXcherry vector has SSTR2 gene under the control of the human cytomegalovirus immediate-early promoter (Pcmv) incorporated in place of the early E1 gene region (ΔE1). Ad5/3Δ24pIXcherry serves as E3-deleted control CRAd lacking SSTR2 transgene.

the analytical data acquired in the context of the expending repertoire of oncolytic virotherapy trials.

Materials and Methods

Cells

The 293 human kidney cell line transformed with Ad5 DNA was purchased from Microbix (Toronto, Ontario). The 911 human embryonic retinoblasts derived by transformation with a plasmid containing 79 to 5,789 basepairs of the Ad5 genome[31] were obtained through Crucell Holland B.V. (Leiden, the Netherlands). The human ovarian carcinoma cell line SKOV3.ip1 was obtained from Janet Price (MD Anderson Cancer Center, Houston, TX). The derivation of a human non–small cell lung cancer line, A-427#7, stably transfected with a hemagglutinin-tagged human SSTR2, was described previously.[32] All cell lines were grown at 37°C in media recommended by the suppliers in a humidified atmosphere of 5% CO_2.

Construction of Ad Vectors

The construction of Ad5/3Δ24 CRAd, which contains a 24-nucleotide deletion from basepair 923 to 946 corresponding to the amino acid sequence 122 LTCHEAGF129 of the E1A protein necessary for Rb protein binding[14] and has the Ad serotype 3 knob domain incorporated into the Ad5 fiber, was described previously.[19,22] The Ad5/3Δ24 CRAd was engineered to encode mCherry fluorescent protein fused to the C-terminus of a minor capsid protein IX as described recently,[30] resulting in generation of Ad5/3Δ24pIXcherry CRAd. The genome of Ad5/3Δ24pIXcherry/SSTR CRAd was generated as follows. First, the SSTR2 gene obtained from the pAChSSTr2 plasmid[33] was cloned into pShuttlE3 plasmid[34] between *BamH*I and *Sal*I restriction sites downstream of the kanamycin gene and in the same orientation as the downstream fiber gene, and the resultant plasmid was linearized and used for homologous recombination with pAdEasy-1 rescue plasmid[35] in *Escherichia coli* BJ5183 cells as previously described.[34] The recombinant pAdEasy(E3/SSTR2) plasmid containing both SSTR2 and kanamycin genes incorporated in place of the deleted E3 region was selected using kanamycin. Subsequently, kanamycin was excised with the two surrounding *Swa*I sites, and after self-ligation of pAdEasy(E3/SSTR2) plasmid, it was retransformed into *E. coli* DH10B using ampicillin selection. The Ad5/3Δ24pIXcherry/SSTR genome was generated by homologous recombination between pAdEasy(E3/SSTR2) and pSlΔ24-pIX-mCherry plasmids

essentially as described elsewhere.[30] To construct replication-deficient Ad5/3-SSTRpIXcherry vector, we employed pShSSTR2-IXmCherry plasmid, which was generated by replacing a 1,654-basepair *Sac*II fragment in pShuttle-CMVHAhSSTr2 plasmid[33] with *Sac*II fragment (2,408 base-pairs) isolated from pSlΔ24-pIX-mCherry,[30] for homologous recombination with pAdEasy-1-derived rescue plasmid AdEz-F5/3[30] in *E. coli* BJ5183 cells.

The constructed plasmids containing viral genomes were validated by polymerase chain reaction (PCR), restriction analysis, and partial sequencing and were then linearized with *Pac*I to release the inverted terminal repeats of the viral genomic DNA and then used to transfect 293 cells to rescue Ad5/3Δ24pIXcherry/SSTR CRAd and replication-incompetent Ad5/3-SSTRpIXcherry vector. The newly rescued Ad vectors as well as Ad5/3Δ24pIXcherry and Ad5/3Δ24 CRAd were propagated on 911 cells,[31] purified by centrifugation on CsCl gradients according to standard protocol, and dialyzed against phosphate-buffered saline (PBS) (8 mM Na_2HPO_4, 2 mM KH_2PO_4 [pH 7.4], 137 mM NaCl, 2.7 mM KCl) containing 10% glycerol. The titers of physical viral particles were determined by the methods of Maizel and colleagues.[36] The titers of infectious viral particles were determined by plaque assay using 293 cells as described by Mittereder and colleagues.[37] The ratios of viral particles to plaque-forming units (pfu) determined for Ad5/3Δ24pIXcherry/SSTR, Ad5/3Δ24pIXcherry, Ad5/3Δ24, and Ad5/3-SSTRpIXcherry vector were 37, 29, 25, and 42, respectively.

Indirect Immunofluorescence

We employed mouse monoclonal antibody (mAb) IgG_{2A}, which was generated against intracellular domain of human SSTR2 (amino acids 1–369, Accession # P30874), purchased from Neuromics Antibodies (Edina, MN), to evaluate the SSTR2 expression in SKOV3.ip1 cells infected with generated Ad vectors by indirect immunofluorescence assay using flow cytometry as follows. The SKOV3.ip1cell monolayers grown in a six-well plate (1×10^6 cells/well) were infected with Ad5/3Δ24pIXcherry/SSTR CRAd or replication-incompetent Ad5/3-SSTRpIXcherry vector at a multiplicity of infection (MOI) of 100 viral particles/cell and incubated in culture medium containing 5% fetal bovine serum (FBS) at 37°C in a humidified atmosphere of 5% CO_2 for 24, 36, 48, and 96 hours. Infected and uninfected control (mock) cell monolayers were harvested in 1 mL/monolayer PBS and centrifuged for 5 minutes at 1,000 RPM. Cell pellets were resuspended in 1 mL of ice-cold 70% ethanol and incubated on ice for 2 hours or

overnight to fix soluble intracellular antigens. Cells were aliquoted into 5 mL polystyrene round-bottomed tubes (2.5×10^5 cells/tube) and centrifuged for 5 minutes at 1,500 RPM, and cell pellets were resuspended in 4 mL PBS. This step was repeated to wash away any excess ethanol; cells were resuspended in 125 μL PBS containing 0.1% Triton X-100 and incubated in a 37°C water bath for 15 minutes to permeabilize cell membranes. Cells were centrifuged for 5 minutes at 1,500 RPM, cell pellets were resuspended in 2 mL fluorescent-activated cell sorting (FACS) buffer (PBS containing 0.5% bovine serum albumin [BSA], 0.1% NaN$_3$, 0.1% Triton X-100), and cells were pelleted again. Cells were resuspended at a concentration of 2×10^6 cells/mL in a 100 μL/tube FACS buffer containing human SSTR2 mAb at a concentration of 5 μg/mL and incubated at 4°C for 1 hour using a plate shaker. An isotype-matched normal mouse IgG$_{2A}$ (5 μg/mL) was used as a negative control. Cells were diluted in 4 mL FACS buffer, centrifuged as above, resuspended in FACS buffer containing the secondary Alexa 488–labeled goat antimouse antibody (Molecular Probes, Eugene, OR) at a concentration of 5 μg/mL, and incubated at 4°C for 1 hour using a plate shaker. Cells were washed with FACS buffer by centrifugation as above prior to flow cytometry analysis. Cell samples were analyzed on a BD Biosciences FACSAria (San Jose, CA) using the 488 nm blue laser with the filter set for fluorescein isothiocyanate, and 10^4 events were acquired per each cell specimen. Data were expressed as the geometric mean fluorescence intensity of the entire gated population. The positive cell population was determined by gating the right-hand tail of the distribution of the negative control sample for each time point postinfection at 1%.

Western Blot Analysis

Samples of CsCl-purified Ad vectors were boiled in Laemmli loading buffer, and 1.0×10^9 viral particles of each virus were loaded on a 4 to 20% gradient sodium dodecyl sulfate–polyacrylamide gel electrophoresis (SDS-PAGE) gel (Pierce, Rockford, IL). Electrophoretically resolved viral proteins were transferred to a polyvinylidene fluoride (PVDF) membrane and analyzed for the presence of modified pIX-mCherry or chimeric 5/3 fiber proteins using anti-pIX polyclonal rabbit serum or mAb 4D2 against the fiber tail region, respectively, as we described previously.[38] All primary antibodies were used at a dilution of 1:1,000 for overnight incubation at 4°C. Bound rabbit antibodies and mouse mAb were detected with a secondary goat antirabbit or goat antimouse antibody conjugated

with alkaline phosphatase (Sigma, St. Louis, MO) and developed with an alkaline phosphatase substrate kit (Bio-Rad Laboratories, Hercules, CA).

Analysis of Expression of pIX-mCherry Protein

The SKOV3.ip1cell monolayers grown in a 24-well plate (3×10^5 to 5×10^5 cells/well) were incubated with each Ad vector at an MOI of 0.3, 1.0, and 3 pfu/cell in 200 μL of culture medium containing 2% FBS. The infection medium was aspirated, and then cells were washed with PBS and incubated in phenol red–free medium containing 5% FBS at 37°C to allow reporter gene expression. The fluorescent light intensities in cell monolayers were measured in the multifunctional Synergy HT plate reader (Bio-Tek Instruments, Winooski, VT) using 560 nm emission and 620 nm excitation filters. The data are presented as relative fluorescent units (RFUs) detected on days 2, 3, 4, 5, 6, and 7 postinfection in triplicate infected cells after the background light signal detected in uninfected cells was subtracted.

Analysis of Oncolytic CRAd Effects

Monolayers of SKOV3ip.1 cells grown in 96-well plates (3×10^3 to 5×10^3 cells/well) were infected in triplicate with Ad5/3Δ24pIXcherry/SSTR, Ad5/3Δ24pIXcherry, and Ad5/3Δ24 CRAd or control replication-deficient Ad5/3-SSTRpIXcherry vector at MOI values ranging from 0.015 to 15 pfu/cell. The decrease in cell viability due to the virus-induced cell killing was measured 7 days postinfection using the Cell Proliferation Assay (Promega Corporation, Madison, WI) as recommended by the manufacturer. Assay was performed by adding 10 μL CellTiter 96 AQ$_{ueous}$ One Solution Reagent directly to culture wells containing red phenol red–free medium supplemented with 2% FBS, incubating for 2 hours, and then recording the absorbance at 490 nm with a plate reader (Synergy HT, Bio-Tek Instruments). The data are presented as the percentages of viable cells in monolayers infected with each viral dose that were determined with respect to the uninfected control set as 100%. To assess the cytopathic effects induced by virus propagation, SKOV3.ip1cells grown in a 24-well plate (3×10^5 to 5×10^5 cells/well) were infected in triplicate with each Ad vector at MOI values ranging from 0.015 to 15 pfu/cell. Plates were incubated for 7 days at 37°C, and the cell monolayer integrity was assessed by staining attached cells with crystal violet and then scanning wells using a Synergy HT plate reader (Bio-Tek Instruments) set at 565 nm. The absorbance values detected in monolayers infected with each viral dose were used to calculate the percentage of cell density

in infected cell monolayers with respect to the uninfected control.

Competitive Binding Assay

The maximum number of binding sites (B_{max}) values of SKOV3.ip1 cells infected with CRAd or replication-deficient vector expressing SSTR2 were determined by using a competitive binding assay with ^{125}I-Tyr^{11}-SST-14 (PerkinElmer, Boston, MA). To this end, cells were infected with Ad5/3Δ24pIXcherry/SSTR CRAd or Ad5/3-SSTRpIXcherry vector at an MOI of 100 viral particles/cell, and membrane preparations were made 36 hours post-infection as previously described.[39] Protein concentrations were determined using the Pierce Non-Reducing Agent Compatible Kit (Rockford, IL). The membrane preparations were diluted in binding buffer (50 mM Tris-Cl [pH 7.4], 5 mM $MgCl_2$, 0.1% BSA, 0.5 mg/mL aprotinin, 200 mg/mL bacitracin, 10 mg/mL leupeptin, 10 mg/mL pepstatin) to obtain a concentration of 25 μg per 100 μL. A 96-well Multiscreen Durapore filtration plate (Millipore, Bedford, MA) pretreated with 0.1% polyethyleneimine via vacuum manifold aspiration was then washed with 300 μL of wash buffer (10 mM HEPES, 1 mM ethylenediaminetetraacetic acid [EDTA], 5 mM $MgCl_2$, 0.1% BSA) before adding 100 μL of each membrane preparation in triplicate per concentration of blocking reagent. The wells were then washed three times with wash buffer. Various concentrations of Tyr^{11}-SST-14 (Bachem, Torrance, CA) blocking reagent, ranging from 0.01 to 55 nM, were then added to the wells in triplicate in a volume of 10 μL for both Ad5/3Δ24pIXcherry/SSTR and Ad5/3-SSTRpIXcherry membrane preparation. ^{125}I-Tyr^{11}-SST-14 ligand (PerkinElmer) was diluted in binding buffer to ≈ 0.04 nM (≈ 10,000 CPM per 100 μL), which was then added to each well. The blocking reagent and radioligand were incubated with shaking for 1 hour at room temperature. All wells were washed twice with wash buffer, and all remaining liquid was removed via vacuum manifold. The membranes, once dry, were placed in individual tubes, and the bound radioactivity was determined using a Packard II gamma counter (PerkinElmer). The data were entered into GraphPad *Prism 4* (La Jolla, CA) to generate homologous competitive binding curves using the one-site homologous competition with depletion equation, and B_{max} values were calculated from the curves.

Biodistribution

All animal studies were performed in accordance with the Guidelines for the Care and Use of Research Animals

approved by the Animal Studies Committee at Washington University. Homozygous Nude-Foxn1 nu/nu female athymic nude mice (Harlan Laboratories, Indianapolis, IN), approximately 6 to 8 weeks of age, were subcutaneously implanted on the rear right and left flanks with SKOV3.ip1 cells, 10^7 cells per injection. Approximately 2 weeks following implantation, tumor volumes reached 0.5 to 1 cm^3 and the animals were randomized based on size to form three groups ($n = 12$ mice per group) and injected intratumorally with 3×10^{10} viral particles/tumor of Ad5/3-SSTRpIXcherry, Ad5/3Δ24pIXcherry/SSTR, or Ad5/3Δ24pIXcherry. Injections of ^{64}Cu-CB-TE2A-Y3-TATE (185 kBq, 5 μCi, 5 ng), which was prepared according to standard literature protocols,[40,41] were performed via the tail vein in five mice from each group on days 4 and 8 following the virus admimistration, and the animals were then sacrificed 4 hours following injection. The blood, liver, kidney, spleen, pancreas, adrenals, muscle, bone, tail, and tumor nodules were collected, weighed, and counted in a gamma counter. The percent injected dose per gram (%ID/g) was calculated based on the corrected radioactivity for each sample compared to a standard, which was representative of the injected dose.

Optical Imaging

Mice bearing subcutaneous tumor xenografts were injected with Ad5/3-SSTRpIXcherry, Ad5/3Δ24pIXcherry/SSTR, or Ad5/3Δ24pIXcherry as described above, and five mice from each group were subjected to noninvasive optical imaging of fluorescent light signal. In vivo imaging of the mice was performed with a multimodal imaging system (In-Vivo MS FX Pro, Bruker, Woodridge, CT) 7 days after virus injection. Mice were placed in the imaging chamber (dorsal side down) and maintained with 2% isoflurane gas anesthesia at a flow rate of approximately 0.5 to 1 L/min per mouse. For mCherry signal detection, multispectral imaging was performed using xenon lamp excitation with 440, 460, 480, 510, 535, and 550 (± 20) nm optical band-pass filters, and emission was captured with a cooled charge-coupled device (CCD) camera after a 600 ± 35 nm band-pass emission filter (em600WA, Bruker). The acquisition time was 10 seconds per image. Spectral separation of MCherry fluorescence from background autofluorescence and region of interest (ROI) analysis were performed using *Molecular Imaging* software (Bruker). Average fluorescence signal from individual tumor ROI were reported in arbitrary units.

Fluorescence microscopy was employed to visualize mCherry-positive cells in the tumor samples extracted from mice 6 days after injection of Ad5/3Δ24pIXcherry/

SSTR or control Ad5/3Δ24pIXcherry CRAd. The samples of tumor tissue were minced using blades, and 30 μL aliquots were placed on glass slides under coverslips (Fisher Scientific, Pittsburgh, PA). Microscopy was performed with an inverted IX-70 fluorescence microscope (Olympus, Melville, NY) equipped with a Magnifire digital CCD camera (Optronics, Goleta, CA). Images were acquired with a ×100 objective using 1-second exposure.

Ad Genome Quantification in Tumors

The tumor nodules that were frozen following biodistribution assay were used to determine virus persistence in tumor xenografts 4 and 8 days after virus injection. The tumor nodules were mechanically homogenized using zirconia/silica beads and Mini-Beadbeater-8 (BioSpec Products, Bartlesville, OK) set at maximum speed during two 30-second intervals. Total DNA was purified from 25 mg of homogenized tumor tissue using a QIAamp DNA Mini Kit (Qiagen, Valencia, CA) as recommended by the manufacturer. The levels of viral genome content were determined in triplicate DNA samples extracted from each tumor by real-time PCR analysis using a Light Cycler 480 System (Roche Diagnostics, Indianapolis, IN) with TaqMan primers and probe designed for the Ad hexon gene. The resultant viral genome copy number was normalized by the amount of cellular DNA, which was determined in the same sample with primers and probe specific for human β-actin (housekeeping gene) using duplexing TaqMan PCR settings.

MicroPET/CT Imaging Studies

Mice were implanted with SKOV3ip.1 tumors on the axillary thorax and allowed to grow as described above. The mice ($n = 3$) were injected intratumorally with 3×10^{10} viral particles/tumor of Ad5/3Δ24pIXcherry/SSTR or Ad5/3Δ24pIXcherry followed by intravenous injection of ^{64}Cu-CB-TE2A-Y3-TATE 4 days later (4.1 MBq [110 μCi]; 175 ng). One and 4 hours after injection, the mice were anesthetized with 1 to 2% isoflurane, positioned supine, and imaged on microPET FOCUS 220 or Inveon PET small-animal scanners (Siemens Medical Solutions, Malvern, PA). The PET acquisition times were 10 minutes. The images were reconstructed with an ordered-subset estimation maximization (OSEM) algorithm, which included corrections for scatter and attenuation. ROI were drawn to encompass the entire tumor to determine the maximum activity concentration (nCi/cc) in the tumor. To calculate the standardized uptake values (SUVs), the nCi/cc was

divided by the nCi injected (decay corrected to the scan start time) and multiplied by the mouse weight.

Statistical Analysis

All data are presented as the mean ± SD. The Student two-tailed *t*-test was used to determine statistical significance at the 95% confidence level, with $p \leq 0.05$ being considered significantly different.

Results

Construction and Molecular Validation of Ad Vectors

In the current study, we designed and constructed four vectors, which are illustrated in Figure 1. The previously described Ad5/3Δ24 CRAd[19] was engineered to encode mCherry fluorescent protein fused to the C-terminus of a minor capsid protein IX as well as SSTR2 transgene incorporated in place of the deleted E3 region. This newly generated Ad5/3Δ24pIXcherry/SSTR CRAd containing two imaging reporters was used along with control vectors to validate our hypothesis. The parental Ad5/3Δ24 CRAd and its pIX-modified derivative, Ad5/3Δ24pIXcherry, which was generated as described previously,[30] were employed as control CRAds (see Figure 1) lacking either both transgenes or SSTR2, respectively. To evaluate if an oncolytic effect of CRAd can interfere with expression of encoded imaging transgenes in infected cells, we constructed Ad5/3-SSTRpIXcherry vector to serve as a replication-deficient control. Ad5/3-SSTRpIXcherry vector contains pIX-fused mCherry, whereas the SSTR2 gene placed under transcriptional control of cytomegalovirus (CMV) promoter is incorporated in the deleted E1 region (see Figure 1).

To assess the efficiency of incorporation of the fluorescent label into viral capsid, we used Western blot to detect pIX-cherry fusion protein in virus preparations purified by CsCl-gradient centrifugation. As can be seen in Figure 2A, the constructed Ad5/3Δ24pIXcherry/SSTR and Ad5/3-SSTRpIXcherry vectors contain a protein band of similar size to the control Ad5/3Δ24pIXcherry virus. This protein band was developed with anti-pIX polyclonal antibody and corresponds to a molecular mass of 46.8 kDa, as expected for polypeptide IX fused with mCherry. A similar intensity of this band detected in newly generated and control virus samples, which were normalized by viral particle number, indicates a relatively efficient incorporation of fluorescent label into assembled Ad5/3Δ24pIXcherry/SSTR and Ad5/3-SSTRpIXcherry virions compared to the Ad5/3Δ24pIXcherry positive control. A minor protein band
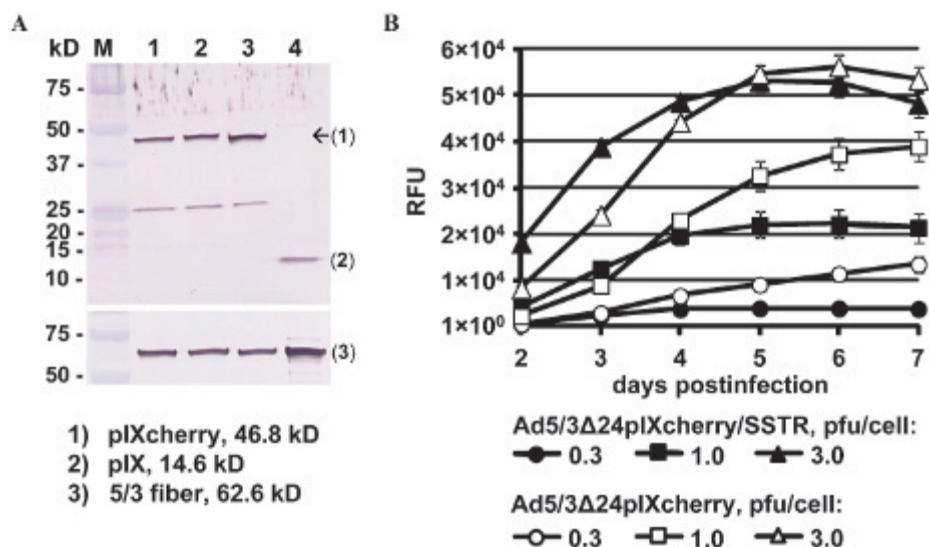
Figure 2. *A*, Analysis of incorporation of pIX-cherry fusion protein into viral capsid. Purified samples of Ad5/3Δ24pIXcherry/SSTR (lane 1), Ad5/3-SSTRpIXcherry (lane 2), Ad5/3Δ24pIXcherry (lane 3), and Ad5/3Δ24 (lane 4) control vector were boiled in Laemmli sample buffer and run on 4 to 20% gradient SDS-PAGE. Viral proteins were transferred to PVDF membrane and incubated with either rabbit antiserum against Ad5 pIX (*top panel*) or 4D2 monoclonal antibody against Ad5 fiber tail (*bottom panel*). Molecular masses of Precision Plus marker proteins (M) are indicated in kilodaltons (kD) on the *left*. *B*, Monitoring of Ad5/3Δ24pIXcherry/SSTR infection in vitro. Monolayers of SKOV3ip.1 cells plated in a 96-well plate were infected with Ad5/3Δ24pIXcherry/SSTR or Ad5/3Δ24pIXcherry CRAd vector at the multiplicity of infection of 0.3, 1, and 3 pfu/cell. The persistence of CRAd in infected cells was monitored for 7 days postinfection based on virus-mediated expression of capsid protein IX fused with the C-terminal mCherry fluorescent protein. The fluorescent light intensity was measured with a plate reader using 560 nm emission and 620 nm excitation filters, and relative fluorescent units (RFU) detected in infected cells are presented after subtracting the background light signal detected in uninfected cells. Each data point represents the cumulative mean ± SD (some error bars are smaller than the symbols).

(approximately 25 kDa), which was detected in all three pIX-modified viruses, appears to represent the proteolytic degradation of pIX-cherry fusion protein due to the presence of adenoviral protease cleavage site within fluorescent protein sequence, as we described previously.[42]

Analysis of Ad-Mediated Expression of pIX-mCherry Fusion

The capacity of pIX-fused mCherry protein to serve as a reporter for optical imaging of Ad amplification was evaluated by infecting the human ovarian cancer cell line SKOV3.ip1 with CRAd or replication-incompetent Ad vector encoding pIX-cherry and measuring fluorescent light intensity at various time points postinfection using a plate reader. Figure 2B illustrates the time course of fluorescent signal development in cell monolayers infected at various MOI with either Ad5/3Δ24pIXcherry/SSTR or control Ad5/3Δ24pIXcherry CRAd. Both CRAd vectors demonstrated a consistent increase in fluorescent light intensity, which correlated with virus amplification and spread of the viral progeny throughout the cell monolayer. Fluorescent cells were observed in SKOV3.ip1 cell monolayers infected with nonreplicating Ad5/3-SSTRpIXcherry

vector; however, due to a lack of virus amplification, the overall signal intensity was very low and could not be distinguished from background autofluorescence (data not shown). We noticed the significant increase in fluorescent signal mediated by Ad5/3Δ24pIXcherry control at later time points (MOI of 0.3 and 1.0 pfu/cell) and early time points (MOI of 3 pfu/cell) postinfection compared to Ad5/3Δ24pIXcherry/SSTR, which can be attributed to higher pIX-cherry expression due to more efficient Ad5/3Δ24-pIXcherry amplification. These data are consistent with our previous reports[29,30,42] and demonstrate the utility of viral capsid labeling with fluorescent tags for identification of infected cells and real-time analysis of CRAd amplification dynamics to allow noninvasive monitoring of oncolytic virus spread by an optical imaging approach.

Analyses of Ad-Mediated SSTR2 Gene Expression

To compare the SSTR2 expression mediated by CRAd and replication-deficient Ad, we carried out flow cytometry with antibody against intracellular SSTR2 domain to assess the overall SSTR2 levels in SKOV3.ip1 cells at various times postinfection. As shown in Figure 3A, both Ad5/3Δ24pIXcherry/SSTR and Ad5/3-SSTRpIXcherry vector
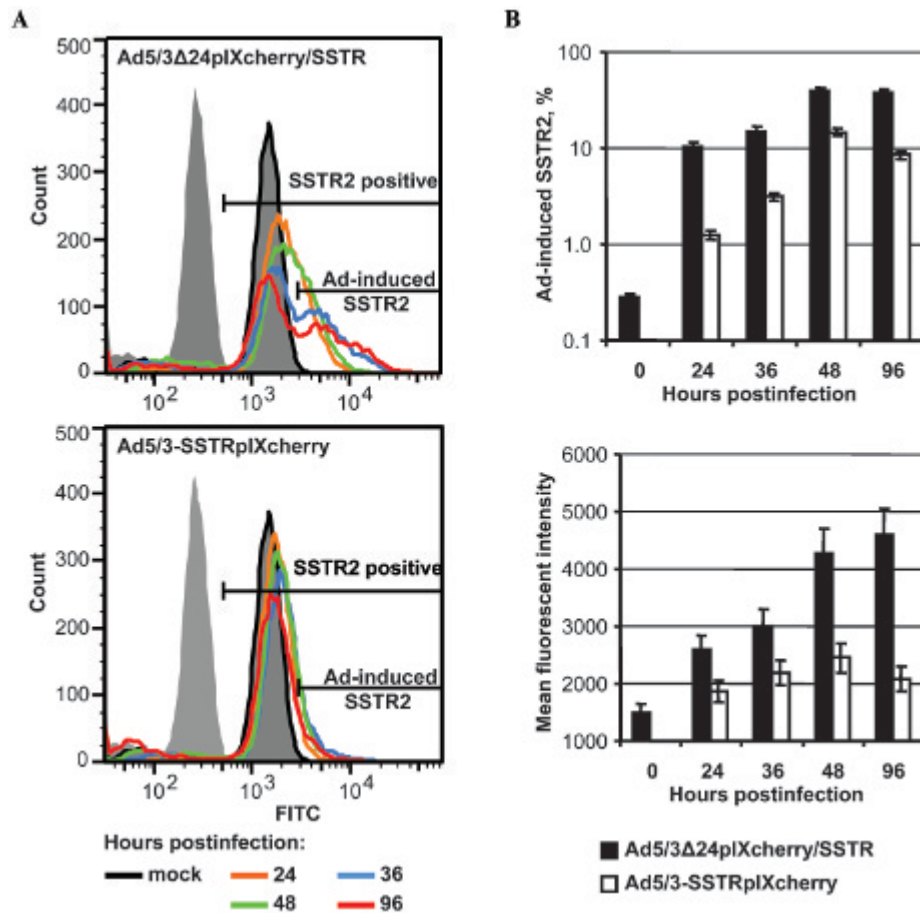
Figure 3. Time course of virus-mediated expression of SSTR2 protein. SKOV3ip.1 cells were infected with 100 viral particles/cell of Ad5/3Δ24pIXcherry/SSTR or Ad5/3-SSTRpIXcherry vector and were analyzed by flow cytometry at various time points postinfection for the levels of SSTR2 expression. Cells were harvested at the indicated time points, fixed, permeabilized, and incubated with primary monoclonal antibody against intracellular SSTR2 domain or mouse IgG isotype control followed by the secondary Alexa 488–labeled antimouse antibody and FACS assay. *A*, Flow cytometry histogram overlays show an increase in the mean fluorescence detected in SKOV3ip.1 cells due to the increase in SSTR2 expression level 24 (*orange*), 36 (*green*), 48 (*blue*), and 96 (*red line*) hours postinfection with Ad5/3Δ24pIXcherry/SSTR (*upper panel*) or Ad5/3-SSTRpIXcherry vector (*lower panel*) compared to the mock-infected cell control (*black line*). *B*, Quantification of the percentage of SKOV3ip.1 cells showing increased expression of SSTR2 protein (*upper panel*) based on increased mean fluorescent intensity levels (*lower panel*) determined at 24, 36, 48, and 96 hours postinfection with Ad5/3Δ24pIXcherry/SSTR or Ad5/3-SSTRpIXcherry vector. FITC = fluorescein isothiocyanate.

provided the highest percentages of SSTR2-positive cells at 48 to 96 hours postinfection. Although both vectors showed a marked increase in SSTR2 expression compared to the background level detected in uninfected SKOV3.ip1, infection with Ad5/3Δ24pIXcherry/SSTR CRAd resulted in a 2.6- to 8.3-fold higher percentage of SSTR2-overexpressing cells, with significantly increased mean fluorescent intensity, compared to Ad5/3-SSTRpIXcherry vector (Figure 3B). This overall augmentation of SSTR2 expression achieved by Ad5/3Δ24pIXcherry/SSTR with respect to Ad5/3-SSTRpIXcherry vector can be attributed to an SSTR2 gene copy number increase due to replication of the CRAd genome in infected SKOV3.ip1 cells.

To examine the SST-binging capacity of SSTR2 overexpressed via CRAd or nonreplicating Ad infection, we carried out competitive binding assays. To this end, we used cellular membranes isolated 36 hours postinfection of SKOV3.ip1 cells infected with 100 viral particles/cell of Ad5/3Δ24pIXcherry/SSTR, Ad5/3-SSTRpIXcherry, and various control vectors to measure binding with ^{125}I-labeled Tyr[11]-SST-14 analogue in the presence or absence of unlabeled Tyr[11]-SST-14 blocking peptide.[39] As shown in

Figure 4A, the detected binding level to the membranes of Ad5/3Δ24pIXcherry/SSTR-infected cells was equivalent to the A427-7 cell line derived to overexpress SSTR2[32] and two times higher compared to Ad5/3-SSTRpIXcherry-infected cells. These binding signals were proven to be SSTR2 specific as they were blocked by unlabeled Tyr[11]-SST-14 peptide to the background level (see Figure 4A) detected in mock-infected cells or cells infected with control Ad vectors that did not contain the SSTR2 gene. In addition, the expression levels of SSTR2 quantified in cells infected with either Ad5/3Δ24pIXcherry/SSTR or Ad5/3-SSTRpIXcherry were calculated as B_{max} values of 3.8 pmol/mg and 2.0 pmol/mg, respectively (Figure 4B). These data are in agreement with flow cytometry analysis (see Figure 3) and demonstrate that greater expression of SSTR2 when using the CRAd is translated into almost a twofold increase in the number of functional receptor molecules displayed on the membranes of infected cells compared to the replication-deficient Ad5/3-SSTRpIXcherry. These results indicate that the oncolytic property of Ad5/3Δ24 CRAd does not interfere with the imaging reporter fidelity in vitro.

A

B
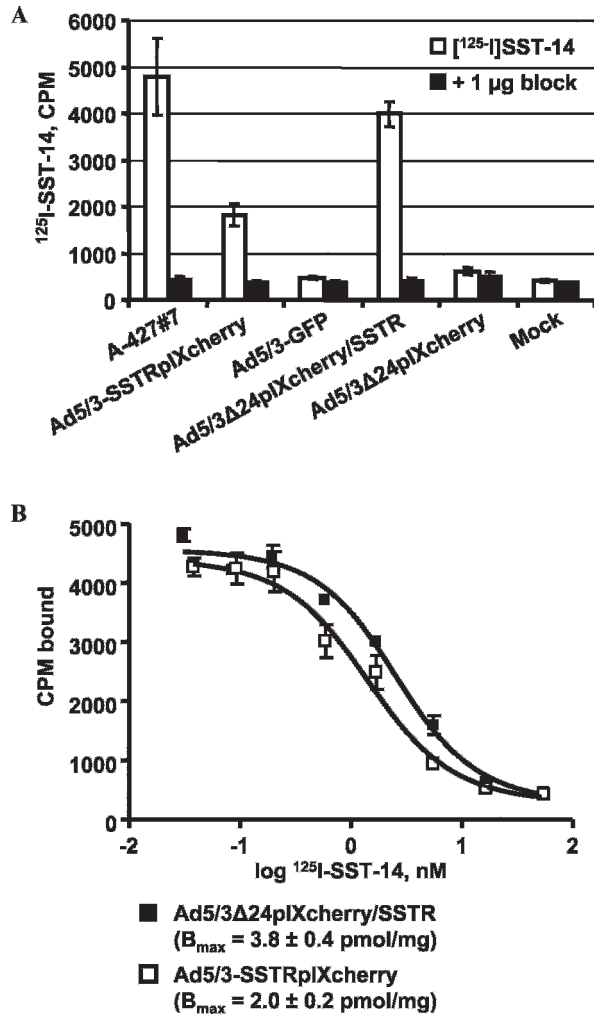
Figure 4. Validation of CRAd to mediate expression of functional SSTR2. *A*, Membrane preparations were made from SKOV3.ip1 cells that were infected 2 days earlier with 100 viral particles/cell of Ad5/SSTRpIXcherry, Ad5/3-GFP, Ad5/3Δ24pIXcherry/SSTR, or Ad5/3Δ24pIXcherry vector. Uninfected cells (mock) were used as a negative control, whereas A-427-7, which stably express SSTR2, were used as a positive control. Binding of ^{125}I-Tyr^{11}-SST-14 to the membranes in the absence or presence of 1 μg of Tyr^{11}-SST-14 as a blocking agent was performed. The data are plotted as the bound counts per minute (CPM) for the mean $\pm$ SD of triplicate measurements. *B*, Representative homologous competitive binding curves using ^{125}I-Tyr^{11}-SST-14 on SKOV3.ip1 cell membranes that had been infected with either Ad5/SSTRpIXcherry or Ad5/3Δ24pIXcherry/SSTR. The data represent the counts per minute of radioligand bound in the presence of various concentrations of block for triplicate data points $\pm$ SD.

Evaluation of Oncolytic Effects of CRAd Vectors In Vitro

The oncolytic effects of Ad5/3Δ24pIXcherry/SSTR vector were assessed in SKOV3.ip1 cells with respect to that of Ad5/3Δ24pIXcherry and Ad5/3Δ24 CRAd or replication-deficient Ad5/3-SSTRpIXcherry control vectors by comparing cell viability and cell monolayer integrity 7 days

postinfection. The values of cell viability and density were determined at various MOI and presented in Figure 5 show the somewhat reduced cytopathic effects of Ad5/3Δ24pIXcherry/SSTR compared to Ad5/3Δ24pIXcherry control and more significant loss of cytotoxicity with respect to the parental Ad5/3Δ24 CRAd. This assay demonstrated that transgene incorporation into viral genome combined with capsid protein IX modification to express imaging reporters may negatively affect the oncolytic potency of CRAd vector.

Detection of SSTR2 Expression Following Intratumoral Virus Injection

The utility of our dual imaging approach to detect CRAd vector localization and persistence in vivo was evaluated in a mouse model of subcutaneous tumor xenografts established using SKOV3.ip1 ovarian cancer cells as described previously.[43] To detect virus-mediated SSTR2 expression, we analyzed systemic biodistribution of ^{64}Cu-CB-TE2A-Y3-TATE ligand 4 and 8 days following intratumoral injection of Ad5/3Δ24pIXcherry/SSTR, Ad5/3Δ24pIXcherry CRAd, or replication-deficient Ad5/3-SSTRpIXcherry vector. Figure 6, A and B, illustrates the radioactivity distribution between various organs and tissues collected 4 hours after intravenous administration of radiolabeled SST analogue, which has been carried out 4 and 8 days subsequent to virus injections. As can be seen in Figure 6, C and D, the levels of ^{64}Cu-CB-TE2A-Y3-TATE uptake detected in tumors injected with either virus were somewhat higher on day 4 than on day 8. Figure 6C shows the significantly greater ($p \leq .05$) radioligand uptake by tumors injected with either Ad5/3-SSTRpIXcherry (3.63 $\pm$ 2.45 %ID/g on day 4 and 2.88 $\pm$ 1.52 %ID/g on day 8) or Ad5/3Δ24pIXcherry/SSTR (2.93 $\pm$ 0.82 %ID/g on day 4 and 1.82 $\pm$ 0.63 %ID/g on day 8) compared to the background level detected in Ad5/3Δ24pIXcherry-injected tumors (1.27 $\pm$ 0.22 %ID/g on day 4 and 0.83 $\pm$ 0.25 %ID/g on day 8). Thus, these data indicate that the specific uptake of radiolabeled ligand was observed at both time points in tumors injected with Ad5/3-SSTRpIXcherry and Ad5/3Δ24pIXcherry/SSTR vectors expressing SSTR2 but not with Ad5/3Δ24pIXcherry control (see Figure 6, C and D). Although it was not statistically significant, somewhat lower radioligand uptake was detected in tumors that were injected with Ad5/3Δ24pIXcherry/SSTR CRAd compared to replication-incompetent Ad5/3-SSTRpIXcherry vector on days 4 ($p = .43$) and 8 ($p = .07$). Interestingly, these results did not correlate with improved radioligand binding to the cells infected with CRAd compared
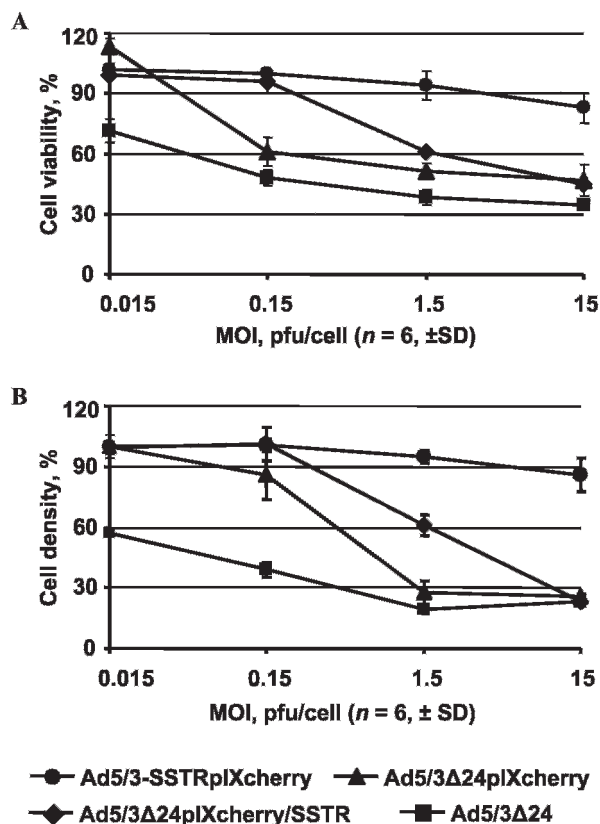
Figure 5. Analysis of oncolytic effects of Ad5/3Δ24pIXcherry/SSTR vector. Monolayers of SKOV3ip.1 cells plated in a 96-well plate were infected with Ad5/3Δ24pIXcherry/SSTR, Ad5/3Δ24pIXcherry, and Ad5/3Δ24 CRAd or control replication-deficient Ad5/3-SSTRpIXcherry vector at the indicated multiplicities of infection (MOIs). The oncolytic effects of CRAd vectors were assessed by determining cell viability and cell monolayer integrity 7 days postinfection. *A*, The virus-induced cell killing was measured using cell proliferation assay by recording absorbance at 490 nm with a 96-well plate reader. The data are presented as the percentages of viable cells in monolayers infected with each viral dose that were determined with respect to the uninfected control set as 100%. *B*, The integrity of cell monolayers was determined by staining adherent cells with crystal violet. The stained monolayers were scanned using a plate reader set at 565 nm to calculate the percentage of cell density in monolayers infected with each viral dose that were determined with respect to the uninfected control. Each data point represents mean ± SD (some error bars are smaller than the symbols).

to replication-incompetent vector expressing SSTR2 that was observed in vitro (see Figure 4B).

Noninvasive Optical Imaging of Intratumoral CRAd Amplification

To evaluate virus replication and spread within the tumors in vivo, we employed noninvasive optical imaging to detect fluorescent light signal 7 days after administration of Ad vector particles labeled with mCherry protein. As can be seen

in Figure 7A, the fluorescent signal generated by replication-deficient Ad5/3-SSTRpIXcherry vector was localized in a single spot within the tumor, whereas injection with Ad5/3Δ24pIXcherry/SSTR and Ad5/3Δ24pIXcherry CRAd resulted in markedly increased fluorescent area and intensity in a majority of the tumors. This observation strongly suggests that efficient replication of CRAd vectors occurred during the 7 days following virus administration and resulted in virus amplification wherein viral progeny could be detected by spectral imaging compared to a nonreplicating Ad5/3-SSTRpIXcherry control. The mean fluorescent light intensity was calculated based on images acquired at different wavelengths, and the data presented in Figure 7B show that fluorescent signal generated in Ad5/3Δ24-pIXcherry/SSTR-injected tumors was amplified 5.3-fold compared to the tumors injected with replication-deficient vector ($p = .018$). The control Ad5/3Δ24pIXcherry CRAd showed 2.6-fold enhanced fluorescent signal compared to nonreplicating vector ($p = .04$) and somewhat lower fluorescence than Ad5/3Δ24pIXcherry/SSTR CRAd (not statistically significant, $p = .15$).

Ad Genome Quantification in Tumors

We used quantitative TaqMan real-time PCR to assess the viral genome copy numbers in tumors harvested for radioligand biodistribution assay. As illustrated in Figure 8, the copy number of both CRAd genomes detected in tumors at 4 and 8 days postinjection was markedly increased compared to the replication-deficient Ad5/3-SSTRpIXcherry control. However, the number of Ad5/3Δ24pIXcherry/SSTR CRAd and nonreplicating Ad5/3-SSTRpIXcherry genomes was decreased sixfold from days 4 to 8 ($p = .009$), whereas the amount of Ad5/3Δ24pIXcherry CRAd remained the same. This assay showed at least fivefold amplification of Ad5/3Δ24pIXcherry/SSTR CRAd compared to nonreplicating Ad5/3-SSTRpIXcherry vector ($p = .008$) at both time points, which correlates with a 5.3-fold increase in fluorescent light signal generated by Ad5/3Δ24pIXcherry/SSTR CRAd relative to the nonreplicating control observed on day 7 postinjection (see Figure 7B). These data clearly demonstrate a superior CRAd vector persistence subsequent to intratumoral administration with respect to replication-incompetent Ad.

PET Imaging of Ad5/3Δ24pIXcherry/SSTR CRAd

To test whether SSTR2 gene transfer could be used to image CRAd vector in vivo, the mice were injected intratumorally with Ad5/3Δ24pIXcherry/SSTR or Ad5/
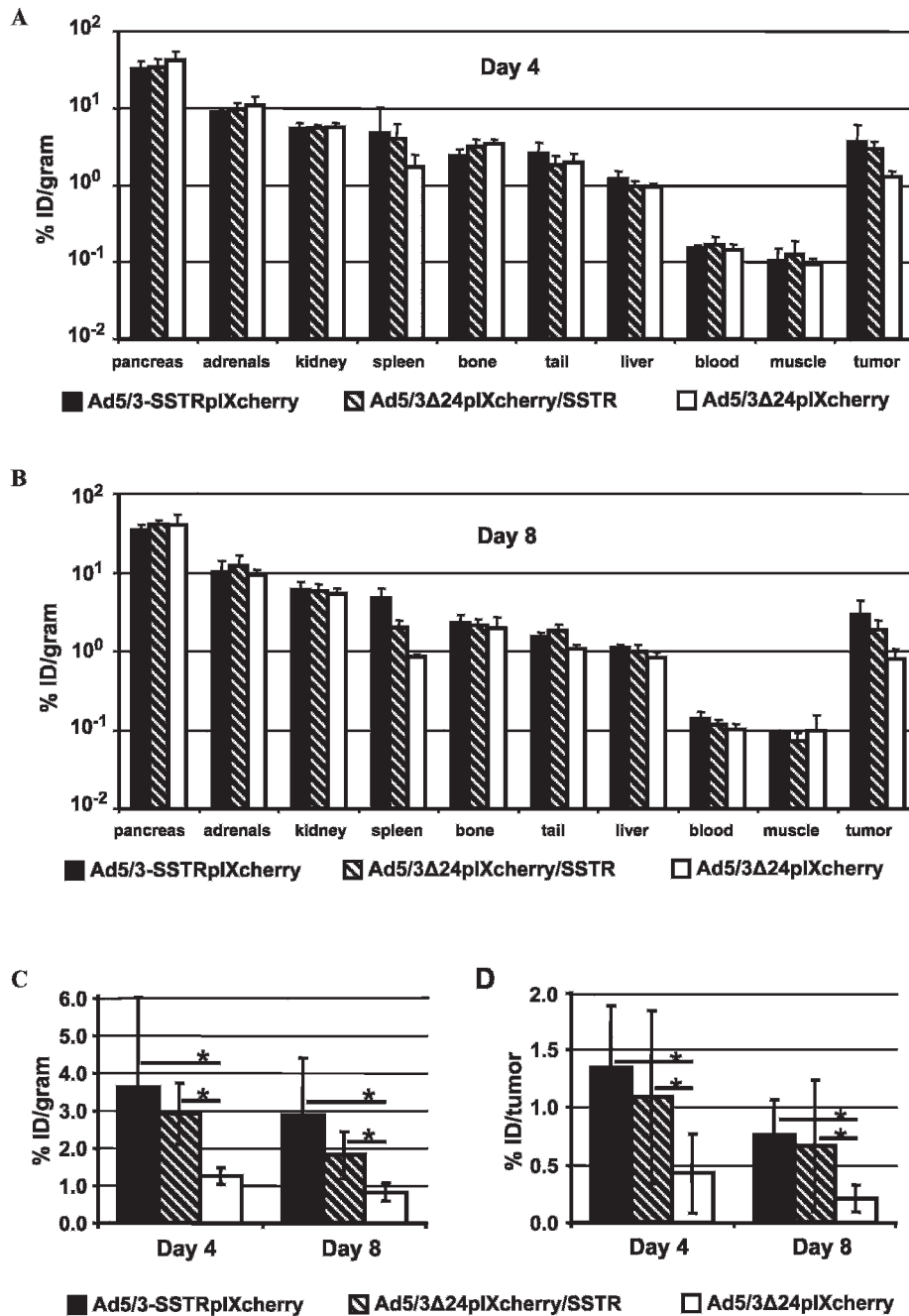
Figure 6. Biodistribution of ^{64}Cu-CB-TE2A-Y3-TATE in mice bearing subcutaneous tumor xenografts. Subcutaneous tumor xenografts established on the rear flank of a female nude mouse using SKOV3.ip1 cells were directly injected with equal doses (3×10^{10} viral particles/tumor) of Ad5/3-SSTRpIXcherry, Ad5/3Δ24pIXcherry/SSTR, or Ad5/3Δ24pIXcherry vector. ^{64}Cu-CB-TE2A-Y3-TATE (5 μCi) was injected via the tail vein 4 or 8 days later, and mice were sacrificed in 4 hours ($n = 5$ for each group) to determine the biodistribution of radioactivity. The data are presented as the %ID/g ± SD detected in the indicated organs and tumors 4 (A) and 8 (B) days following virus administration. *C*, Analysis of the tumor uptake of ^{64}Cu-CB-TE2A-Y3-TATE is shown. Each bar represents the cumulative mean % ID/g ± SD (*$p \leq$ .05). *D*, Analysis of the ^{64}Cu-CB-TE2A-Y3-TATE uptake per tumor is shown. Each bar represents the cumulative mean % ID/tumor ± SD (*$p \leq$ .05).

3Δ24pIXcherry vector. MicroPET/computed tomography (CT) revealed tumor accumulation of ^{64}Cu-CB-TE2A-Y3-TATE 1 hour postinjection in tumors injected with Ad5/3Δ24pIXcherry/SSTR vector 4 days earlier. The small-animal PET/CT images presented in Figure 9A show that SSTR2 ligand uptake is observed in the tumors that received Ad5/3Δ24pIXcherry/SSTR CRAd, whereas tumors that were injected with Ad5/3Δ24pIXcherry CRAd serving as a negative control did not show distinguishable uptake. Clearance of ^{64}Cu-CB-TE2A-Y3-TATE is observed through

the liver and kidneys, which match the biodistribution results. Figure 9B shows the SUV analysis from the PET/CT studies. We observed a 2.1-fold increase in ^{64}Cu-CB-TE2A-Y3-TATE uptake in the tumors that were injected with Ad5/3Δ24pIXcherry/SSTR vector compared to the background uptake detected in tumors injected with Ad5/3Δ24pIXcherry control, respectively. Although these data show that we can visualize radioactive uptake in Ad5/3Δ24pIXcherry/SSTR-injected tumors compared to negative control CRAd in individual animals, and the trend was for greater uptake by
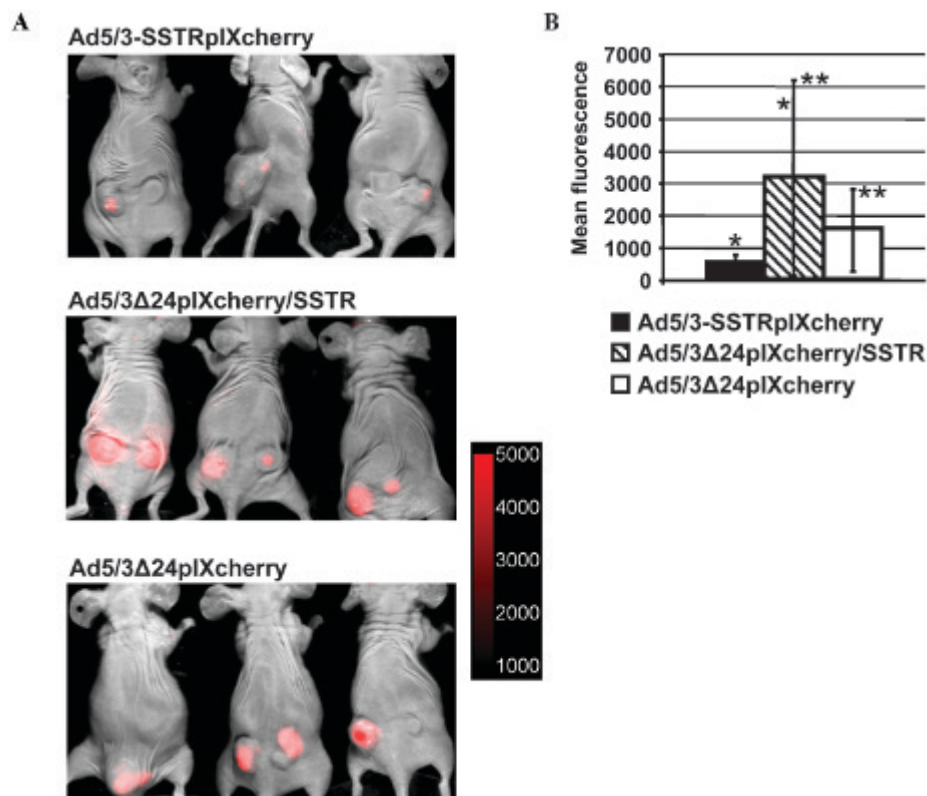
Figure 7. Noninvasive CRAd detection with spectral imaging following intratumoral virus administration. Subcutaneous tumor xenografts were established on both rear flanks of each female nude mouse using SKOV3.ip1 cells and were directly injected with equal doses (3×10^{10} viral particles/tumor) of Ad5/3-SSTRpIXcherry, Ad5/3Δ24pIXcherry/SSTR, or Ad5/3Δ24pIXcherry vector. *A*, Sample images of three mice that received the same Ad vector are shown to illustrate signal variability between different tumors and Ad vectors 7 days postinjection. *B*, Light signals on original unsaturated fluorescent images were quantified using *Molecular Imaging* software, and integrated density was determined for each tumor. Each bar represents the cumulative mean ± SD ($*p < .05$, $**p > .05$).

SUV analysis in the Ad5/3Δ24pIXcherry/SSTR-injected tumors, this difference did not reach statistical significance ($p = .11$). To verify the presence of Ad vectors in tumors, which did not show significant uptake of ^{64}Cu-CB-TE2A-Y3-TATE, we used fluorescence microscopy to detect mCherry-positive cells in the samples of tumor tissue extracted from mice 6 days later. We were able to visualize the fluorescent cells in the tumors injected with Ad5/3Δ24pIXcherry/SSTR or control Ad5/3Δ24pIXcherry CRAd vector (Figure S1, online version only).

Discussion

The biological basis of the CRAd's antineoplastic effect is target cell selective replication whereby direct oncolysis achieves specific tumor cell killing. Progeny virions generated in this process may thereby maintain the replicative cycle via lateral infection of adjoining tumor cells. This novel paradigm of amplification has rationalized the rapid translation of CRAd agents to the context of human clinical trials for a variety of neoplastic disease targets. In the aggregate, these human studies have highlighted the overall safety of CRAd-based interventions. On the other hand, very little information has derived from these trials indicative of valid clinical efficacy. More significantly, the absence of useful surrogate end points in these human studies has further limited any insights into the biological factors confounding CRAd function in the context of human clinical employ.

The mandate to realize surrogate end points in the context of human clinical trials with CRAd agents has thus suggested the utility of imaging analysis. In theory, this
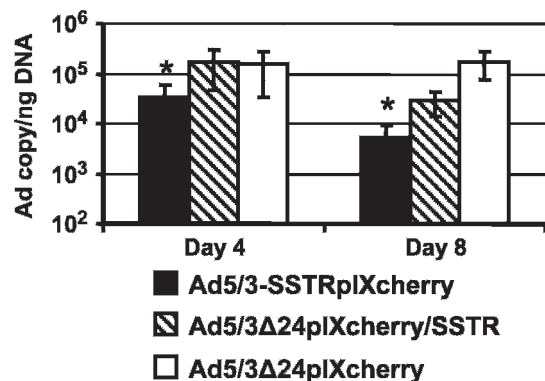
Figure 8. Ad genome quantification in tumors. Total DNA isolated from each tumor sample was analyzed by real-time PCR with primers and probe specific for the hexon gene and then normalized to the amount of cellular DNA detected in the same sample with primers and probe for human β-actin (housekeeping gene) using duplexing TaqMan PCR settings. Each bar represents the cumulative mean Ad genome copy number/ng β-actin DNA ± SD ($*p ≤ .05$).
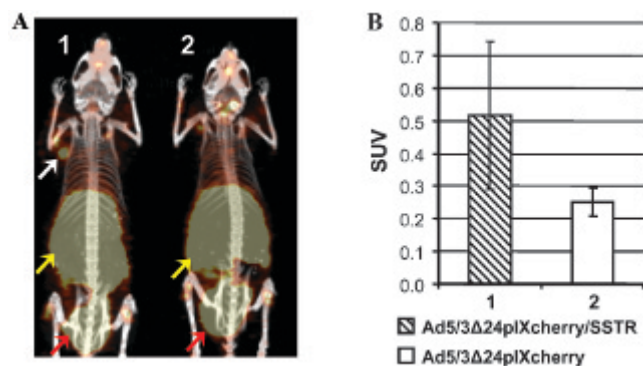
Figure 9. *A*, Representative views of maximum-intensity projections of PET images with coregistered computed tomography of mice bearing SKOV3.ip1 tumors following ^{64}Cu-CB-TE2A-Y3-TATE injection. The images show uptake of ^{64}Cu-CB-TE2A-Y3-TATE in the tumors injected 4 days earlier with Ad5/3Δ24pIXcherry/SSTR CRAd (1) but not in the control tumors injected with Ad5/3Δ24pIXcherry (2). The *white arrows* indicate the location of the tumors, the *red arrows* indicate radioactive excretion through the bladder, and the *yellow arrows* indicate radioactivity clearance via the liver and kidneys. *B*, The standardized uptake value (SUV) analysis for the tumors injected ($n = 3$) with Ad5/3Δ24pIXcherry/SSTR and control Ad5/3Δ24pIXcherry CRAd. Each bar represents the cumulative mean ± SD ($p = .11$).

type of assay could provide critical information with respect to CRAd replication, amplification, and localization. These types of studies could thereby provide key insight into CRAd function in a human clinical context. On this basis, it can be understood that the key attributes of a monitoring system for CRAds would embody the following capacities: (1) direct and dynamic readout of viral replication, (2) direct and dynamic detection of viral spread/lateralization, and (3) noninvasive imaging readout capacity. Of note, these capacities must be achieved in the context of not perturbing the virion's essential infectious activity, which provides the basis for CRAd antitumor potency.

To address this key issue, we developed a novel CRAd vector featuring multimodality imaging capacity, which involves transient SSTR2 reporter gene expression compatible with gamma ray, SPECT, or PET detection and fluorescent labeling based on structural incorporation of mCherry protein into the viral capsid, allowing for optical detection. We hypothesized that this approach would provide the basis for deriving useful surrogate end-point readouts, allowing valid imaging analysis of a human CRAd intervention for carcinoma of the ovary. In this regard, we previously demonstrated the feasibility of using the direct labeling system achievable via genetic fusion of minor capsid protein IX with mRFP1 or mCherry fluorescent protein to dynamically monitor wild-type

Ad5 vector[29] and Ad5/3Δ24 CRAd[30] replication in vivo and to capture the kinetic changes in this process during 20 and 45 days, respectively.

In this study, we validated the utility of genetic pIX-mCherry fusion in the context of our new Ad5/3Δ24pIXcherry/SSTR CRAd to detect virus persistence subsequent to intratumoral administration. Noninvasive whole-body imaging analysis revealed at least a fivefold increase in fluorescent light signal intensity in tumors injected with Ad5/3Δ24pIXcherry/SSTR CRAd compared to replication-incompetent Ad5/3-SSTRpIXcherry vector (see Figure 7B), thereby indicating marked CRAd amplification relative to nonreplicating control during the 7 days following virus administration. This result was confirmed by viral genome quantification in tumors using quantitative real-time PCR and demonstrated a superior CRAd vector persistence subsequent to intratumoral administration with respect to replication-incompetent Ad. We also noted a sixfold decrease in Ad5/3Δ24pIXcherry/SSTR CRAd genome copy number with respect to the control Ad5/3Δ24pIXcherry CRAd on day 8 postinjection (see Figure 8). This decrease was not consistent with an approximate twofold higher light signal, which was detected by noninvasive imaging analysis of intratumoral Ad5/3Δ24pIXcherry/SSTR CRAd amplification compared to the control Ad5/3Δ24pIXcherry CRAd on day 7 postinjection (see Figure 7B). We speculate that the most likely explanation for this inconsistency could be a proteolytic degradation of mCherry protein during proliferation of pIXmCherry-incorporating CRAd in vivo. We detected the proteolytic degradation products of fluorescently labeled pIX-mCherry fusion protein by Western blot analysis of generated viruses (see Figure 2A), which was previously attributed to Ad protease cleavage during capsid assembly due to the presence of consensus recognition sites, (M/I/L)XGX-G and (M/I/L)XGG-X,[44] within fluorescent proteins including enhanced green fluorescent protein and monomeric red fluorescent protein 1.[42] Certain limitations are associated with the use of fluorescence imaging in our genetic capsid labeling system. The detection depth associated with current fluorescence-based optical imaging technology remains limited.[45] Additionally, the possibility of achieving tomographic data from fluorescence imaging for volumetric quantification is still under development and not widely available.[46,47] As a result, conventional fluorescence imaging is presently limited to application for superficial or accessible tumors and would not be adequate for accurate quantification of volumetric fluorescence signals. Despite these shortcomings, optical imaging is less expensive and more convenient than many other imaging modalities and therefore can serve as an attractive alternative in preclinical studies

of fluorescently labeled CRAd because light penetration in small animals is less of a concern than in humans. Our laboratory and others have recently begun to explore the functional utility of modifying Ad tropism for applied human interventional contexts. For these studies, both preclinical and clinical analyses of viral particle biodistribution as well as reporter gene locale and persistence are sought. The capsid label provides a facile means to monitor vector particle biodistribution, as we have shown.[25] Although this method cannot be employed for all cancer contexts where CRAd agents would be employed, we have found this adjunctive reporter to allow the derivation of useful data in the context of our ovarian cancer models. In this regard, alternative imaging reporters that may be more practical for deeper tissue detection, which include firefly luciferase[48] and the herpes simplex virus type 1 thymidine kinase (HSV1-tk) gene,[49] were also considered for genetic capsid labeling.[27,28,50]

Of note, nuclear imaging has received much attention because it is highly quantitative and sensitive and is directly applicable to clinical trials. The HSV1-tk gene and its mutants have been studied extensively and used for PET with various radiolabeled substrates to image gene transfer mediated by replication-deficient Ad vector in mice,[51–54] nonhuman primates,[55] and liver cancer patients.[56] The feasibility of using the HSV1-tk gene to monitor anti-tumoral effects of armed CRAd has recently been demonstrated in a murine model of pancreatic cancer[57] and following direct intrapancreatic virus injection in a preclinical study in a dog model.[58] The sodium iodide symporter (NIS) is one of several human genes that are being developed for nuclear imaging with radioiodide[59] and has been extensively employed for imaging of oncolytic Ad vectors in animal models of human cancer[60–67] and phase I clinical trials in prostate cancer patients by SPECT.[68]

Our group and others have focused on using human SSTR2, a member of the G protein–coupled receptor family, for imaging of gene transfer using gamma camera, SPECT, and PET.[24,69–74] Although both NIS and HSV1-tk derivatives have been investigated for imaging of oncolytic vectors based on herpes virus,[75] vesicular stomatitis virus,[76] vaccinia virus,[77–81] measles virus,[82–87] and Ad[60–68] in vivo, the use of SSTR2 reporter has been limited to replication-deficient Ad[24,69–74] and vaccinia virus[88] to date. To assess the utility of SSTR2 reporter in the context of CRAd vector, we studied whether the oncolytic viral effects can interfere with SSTR2 imaging fidelity by comparing the engineered Ad5/3Δ24pIXcherry/SSTR CRAd and replication-deficient Ad5/3-SSTRpIXcherry control side by side for SSTR2 expression and tracer binding efficiencies in vitro and in vivo.

Analysis of SSTR2 expression showed that Ad5/3Δ24pIXcherry/SSTR infection of SKOV3.ip1 cells resulted in up to eightfold SSTR2 upregulation compared to Ad5/3-SSTRpIXcherry vector (see Figure 3B). The in vitro binding studies showed that SSTR2 was functional as it specifically bound ^{125}I-Tyr[11]-SST-14 tracer, resulting in almost a twofold increase in receptor concentration (B_{max}) observed in cells infected with Ad5/3Δ24pIXcherry/SSTR CRAd compared to Ad5/3-SSTRpIXcherry control (see Figure 4B). Biodistribution studies revealed specific uptake of ^{64}Cu-CB-TE2A-Y3-TATE tracer into SKOV3.ip1 tumors directly injected with Ad5/3Δ24pIXcherry/SSTR or Ad5/3-SSTRpIXcherry vector relative to control tumors injected with Ad5/3Δ24pIXcherry CRAd (see Figure 6, C and D). These studies demonstrated a 2.3- and 2.2-fold increase in tracer uptake in tumors 4 and 7 days after injection with Ad5/3Δ24pIXcherry/SSTR compared to the control Ad5/3Δ24pIXcherry CRAd. Interestingly, these somewhat higher, 2.8- and 3.4-fold, increases in tracer uptake were detected in tumors injected with nonreplicating Ad5/3-SSTRpIXcherry vector (3.6% ID/g on day 4, 2.8% ID/g on day 8) with respect to control tumors. We previously demonstrated similar tumor uptake (1.3% ID/g) 6 hours after injection of ^{111}In-DTPA-D-F1-octreotide in mice bearing A-427 tumors directly injected with replication-deficient AdSSTR2.[70,89] McCart and colleagues reported tumor uptake of approximately 1% ID/g at 4 and 24 hours after injection of ^{111}In-DTPA-D-F1-octreotide in mice that carried subcutaneous MC38 tumors and that had received an intraperitoneal injection of oncolytic vaccinia virus encoding SSTR2 6 days earlier.[88] Yang and colleagues reported that HT1080 tumor xenografts stably expressing SSTR2 had ^{111}In-DTPA-D-F1-octreotide uptake of approximately 1% ID/g 24 hours after injection.[90] Thus, our results are comparable to those of other studies evaluating the uptake of ^{111}In-labeled SST analogues in tumors induced to express SSTR2. Analysis of noninvasive optical imaging, viral genome quantification, and biodistribution data indicates that a twofold increase in SSTR2 concentration mediated by Ad5/3Δ24pIXcherry/SSTR CRAd with respect to Ad5/3-SSTRpIXcherry control in vitro (see Figure 4B), along with superior CRAd persistence observed in vivo (see Figure 7B and Figure 8), did not translate to augmented tracer uptake in tumors injected with CRAd relative to replication-incompetent vector (see Figure 6). Similar to the previous studies,[70,72] there was increased spleen accumulation of ^{64}Cu-CB-TE2A-Y3-TATE after injection of Ad5/3-SSTRpIXcherry or Ad5/3Δ24pIXcherry/SSTR compared to Ad5/3Δ24pIXcherry control. This is likely due to Ad infection of these organs even though virus was injected

intratumorally. Other studies have shown that Ad vectors can "leak" from the tumor after direct intratumoral administration and infect the liver and spleen because of Ad natural tropism for these normal tissues.[91–93]

Although our PET/CT imaging studies demonstrated that Ad5/3Δ24pIXcherry/SSTR-injected tumors can be visualized in individual animals and the trend was for greater radioactive uptake by SUV analysis compared to control CRAd, this difference did not reach statistical significance. Since the magnitude of the differences observed between the experimental and control constructs remains to be a concern for clinical translation, we believe that the radioligand-CRAd combination used in this study may not be the one to move forward into clinical trials and a more optimized combination would be expected to give a better differential. We envision that during clinical application of this technology, imaging would be performed prior to virus administration to determine the baseline uptake. Imaging would then be performed at time points after CRAd administration to determine if significant reporter gene transfer has occurred.

Although SSTR2 was not employed previously for CRAd monitoring, several groups reported the use of human NIS as a reporter gene for imaging of various CRAd agents following intratumoral injection in animal models of colorectal,[63,65] prostate,[60,66,67,94–96] and peritoneal ovarian cancer.[62] These SPECT imaging studies show that human NIS expression reaches a peak 2 to 4 days after intratumoral injection, followed by a sharp disappearance of human NIS–dependent accumulation of radiotracer. A similar kinetic has been reported by Barton and colleagues,[97] using an oncolytic Ad agent armed with two therapeutic suicide genes and the human NIS reporter gene in a recent first phase I trial, which demonstrated that human NIS expression can be measured noninvasively in the human prostate by SPECT.[68] These data are consistent with our PET imaging results and indicate that CRAd presence in tumors can be detected by SPECT/PET during the early stages of virotherapy treatment. However, as viral oncolysis creates tumor destruction, the imaging system fails to correlate with the magnitude of CRAd amplification because intact cells are required for expression of HSV1-tk, human NIS, and SSTR2 reporter gene products and their physiologic protein functions. In the case of fluorescent reporters, it is likely that these proteins will continue to emit fluorescence on stimulation even after release by dead cells.

These studies have demonstrated that each reporter exhibited limited functionality in the CRAd context in vivo, thus suggesting that the use of a proposed dual imaging approach combining both PET and optical CRAd

detection should provide the technical basis of adaption for a range of preclinical and clinical applications. A rationale for combining two different imaging reporters is to exploit the inherent advantages of one modality to compensate for the limitations of another. Despite the fact that nuclear imaging has the advantages of being highly sensitive and quantitative, it is expensive and does not have the resolution for single-cell imaging. Although the sensitivity of optical probes decreases with the depth of tissue, optical imaging is cost-effective and sensitive for surface detection and can be used for single-cell imaging.[98] Therefore, these optical and nuclear imaging reporters can complement each other in preclinical tumor models for the imaging of cancer therapy.[99,100] Our study demonstrated the feasibility of monitoring CRAd persistence and biodistribution using a dual imaging vector strategy in the context of intratumoral virus administration, thus illustrating its utility for advanced CRAd development and suggesting that it could also be applicable for monitoring the effects of CRAd virotherapy in patients via imaging modalities currently available within the clinical setting.

Acknowledgments

References

1. The Journal of Gene Medicine. Gene therapy clinical trials worldwide. Available at: http://www.wiley.com/legacy/wileychi/genmed/clinical (accessed September 2013).
2. Shenk T. Adenoviridae: the viruses and their replication. In: Fields BN, Knipe DM, Howley PM, et al, editors. Fields virology. Vol 2, 3rd ed. Philadelphia: Lippincott-Raven Publishers; 1996. p. 2111–48.
3. Kanerva A, Raki M, Hemminki A. Gene therapy of gynaecological diseases. Expert Opin Biol Ther 2007;7:1347–61, doi:10.1517/14712598.7.9.1347.
4. Kimball KJ, Numnum TM, Rocconi RP, et al. Gene therapy for ovarian cancer. Curr Oncol Rep 2006;8:441–7, doi:10.1007/s11912-006-0073-x.
5. O'Shea CC. Viruses - seeking and destroying the tumor program. Oncogene 2005;24:7640–55, doi:10.1038/sj.onc.1209047.
6. Douglas JT, Kim M, Sumerel LA, et al. Efficient oncolysis by a replicating adenovirus (Ad) in vivo is critically dependent on

tumor expression of primary ad receptors. Cancer Res 2001;61: 813–7.

7. Hemminki A, Kanerva A, Liu B, et al. Modulation of coxsackie-adenovirus receptor expression for increased adenoviral transgene expression. Cancer Res 2003;63:847–53.

8. Kim M, Zinn KR, Barnett BG, et al. The therapeutic efficacy of adenoviral vectors for cancer gene therapy is limited by a low level of primary adenovirus receptors on tumour cells. Eur J Cancer 2002;38:1917–26, doi:10.1016/S0959-8049(02)00131-4.

9. Dmitriev I, Krasnykh V, Miller CR, et al. An adenovirus vector with genetically modified fibers demonstrates expanded tropism via utilization of a coxsackievirus and adenovirus receptor-independent cell entry mechanism. J Virol 1998;72:9706–13.

10. Krasnykh VN, Mikheeva GV, Douglas JT, et al. Generation of recombinant adenovirus vectors with modified fibers for altering viral tropism. J Virol 1996;70:6839–46.

11. Wang H, Li ZY, Liu Y, et al. Desmoglein 2 is a receptor for adenovirus serotypes 3, 7, 11 and 14. Nat Med 2011;17:96–104, doi:10.1038/nm.2270.

12. Kanerva A, Mikheeva GV, Krasnykh V, et al. Targeting adenovirus to the serotype 3 receptor increases gene transfer efficiency to ovarian cancer cells. Clin Cancer Res 2002;8:275–80.

13. Tsuruta Y, Pereboeva L, Breidenbach M, et al. A fiber-modified mesothelin promoter-based conditionally replicating adenovirus for treatment of ovarian cancer. Clin Cancer Res 2008;14:3582–8, doi:10.1158/1078-0432.CCR-07-5053.

14. Fueyo J, Gomez-Manzano C, Alemany R, et al. A mutant oncolytic adenovirus targeting the Rb pathway produces anti-glioma effect in vivo. Oncogene 2000;19:2–12, doi:10.1038/sj.onc.1203251.

15. Heise C, Hermiston T, Johnson L, et al. An adenovirus E1A mutant that demonstrates potent and selective systemic anti-tumoral efficacy. Nat Med 2000;6:1134–9, doi:10.1038/80474.

16. D'Andrilli G, Kumar C, Scambia G, et al. Cell cycle genes in ovarian cancer: steps toward earlier diagnosis and novel therapies. Clin Cancer Res 2004;10:8132–41, doi:10.1158/1078-0432.CCR-04-0886.

17. Lockley M, Fernandez M, Wang Y, et al. Activity of the adenoviral E1A deletion mutant dl922-947 in ovarian cancer: comparison with E1A wild-type viruses, bioluminescence monitoring, and intraperitoneal delivery in icodextrin. Cancer Res 2006;66:989–98, doi:10.1158/0008-5472.CAN-05-2691.

18. Bauerschmitz GJ, Lam JT, Kanerva A, et al. Treatment of ovarian cancer with a tropism modified oncolytic adenovirus. Cancer Res 2002;62:1266–70.

19. Kanerva A, Zinn KR, Chaudhuri TR, et al. Enhanced therapeutic efficacy for ovarian cancer with a serotype 3 receptor-targeted oncolytic adenovirus. Mol Ther 2003;8:449–58, doi:10.1016/S1525-0016(03)00200-4.

20. Zhu ZB, Lu B, Park M, et al. Development of an optimized conditionally replicative adenoviral agent for ovarian cancer. Int J Oncol 2008;32:1179–88.

21. Kimball KJ, Preuss MA, Barnes MN, et al. A phase I study of a tropism-modified conditionally replicative adenovirus for recurrent malignant gynecologic diseases. Clin Cancer Res 2010;16: 5277–87, doi:10.1158/1078-0432.CCR-10-0791.

22. Kim KH, Dmitriev IP, Saddekni S, et al. A phase I clinical trial of Ad5/3-Delta24, a novel serotype-chimeric, infectivity-enhanced, conditionally-replicative adenovirus (CRAd), in patients with recurrent ovarian cancer. Gynecol Oncol 2013;130:518–24, doi:10.1016/j.ygyno.2013.06.003.

23. Blasberg R. PET imaging of gene expression. Eur J Cancer 2002; 38:2137–46, doi:10.1016/S0959-8049(02)00390-8.

24. Kim KH, Dmitriev I, O'Malley JP, et al. A phase I clinical trial of Ad5.SSTR/TK.RGD, a novel infectivity-enhanced bicistronic adenovirus, in patients with recurrent gynecologic cancer. Clin Cancer Res 2012;18:3440–51, doi:10.1158/1078-0432.CCR-11-2852.

25. Le LP, Everts M, Dmitriev IP, et al. Fluorescently labeled adenovirus with pIX-EGFP for vector detection. Mol Imaging 2004;3:105–16, doi:10.1162/1535350041464874.

26. Li J, Fatima A, Komarova S, et al. Evaluation of adenovirus capsid labeling versus transgene expression. Virol J 2010;7:21, doi:10.1186/1743-422X-7-21.

27. Li J, Le L, Sibley DA, et al. Genetic incorporation of HSV-1 thymidine kinase into the adenovirus protein IX for functional display on the virion. Virology 2005;338:247–58, doi:10.1016/j.virol.2005.04.005.

28. Kimball KJ, Rivera AA, Zinn KR, et al. Novel infectivity-enhanced oncolytic adenovirus with a capsid-incorporated dual-imaging moiety for monitoring virotherapy in ovarian cancer. Mol Imaging 2009;8:264–77.

29. Le LP, Le HN, Dmitriev IP, et al. Dynamic monitoring of oncolytic adenovirus in vivo by genetic capsid labeling. J Natl Cancer Inst 2006;98:203–14, doi:10.1093/jnci/djj022.

30. Borovjagin AV, McNally LR, Wang M, et al. Noninvasive monitoring of mRFP1- and mCherry-labeled oncolytic adenoviruses in an orthotopic breast cancer model by spectral imaging. Mol Imaging 2010;9:59–75.

31. Fallaux FJ, Kranenburg O, Cramer SJ, et al. Characterization of 911: a new helper cell line for the titration and propagation of early region 1-deleted adenoviral vectors. Hum Gene Ther 1996;7: 215–22, doi:10.1089/hum.1996.7.2-215.

32. Parry JJ, Eiblmaier M, Andrews R, et al. Characterization of somatostatin receptor subtype 2 expression in stably transfected A-427 human cancer cells. Mol Imaging 2007;6:56–67.

33. Rogers BE, Chaudhuri TR, Reynolds PN, et al. Non-invasive gamma camera imaging of gene transfer using an adenoviral vector encoding an epitope-tagged receptor as a reporter. Gene Ther 2003;10:105–14, doi:10.1038/sj.gt.3301853.

34. Le LP, Le HN, Nelson AR, et al. Core labeling of adenovirus with EGFP. Virology 2006;351:291–302, doi:10.1016/j.virol.2006.03.042.

35. He TC, Zhou S, da Costa LT, et al. A simplified system for generating recombinant adenoviruses. Proc Natl Acad Sci U S A 1998;95:2509–14, doi:10.1073/pnas.95.5.2509.

36. Maizel JV Jr, White DO, Scharff MD. The polypeptides of adenovirus. I. Evidence for multiple protein components in the virion and a comparison of types 2, 7A, and 12. Virology 1968;36: 115–25, doi:10.1016/0042-6822(68)90121-9.

37. Mittereder N, March KL, Trapnell BC. Evaluation of the concentration and bioactivity of adenovirus vectors for gene therapy. J Virol 1996;70:7498–509.

38. Kashentseva EA, Douglas JT, Zinn KR, et al. Targeting of adenovirus serotype 5 pseudotyped with short fiber from serotype 41 to c-erbB2-positive cells using bispecific single-chain diabody. J Mol Biol 2009;388:443–61, doi:10.1016/j.jmb.2009.03.016.

39. Rogers BE, McLean SF, Kirkman RL, et al. In vivo localization of [(111)In]-DTPA-D-Phe1-octreotide to human ovarian tumor xenografts induced to express the somatostatin receptor subtype 2 using an adenoviral vector. Clin Cancer Res 1999;5:383–93.

40. Achilefu S, Wilhelm RR, Jimenez HN, et al. A new method for the synthesis of tri-tert-butyl diethylenetriaminepentaacetic acid and its derivatives. J Org Chem 2000;65:1562–5, doi:10.1021/jo991453t.

41. Sprague JE, Peng Y, Sun X, et al. Preparation and biological evaluation of copper-64-labeled tyr3-octreotate using a cross-bridged macrocyclic chelator. Clin Cancer Res 2004;10:8674–82, doi:10.1158/1078-0432.CCR-04-1084.

42. Ugai H, Wang M, Le LP, et al. In vitro dynamic visualization analysis of fluorescently labeled minor capsid protein IX and core protein V by simultaneous detection. J Mol Biol 2010;395:55–78, doi:10.1016/j.jmb.2009.10.034.

43. Rocconi RP, Zhu ZB, Stoff-Khalili M, et al. Treatment of ovarian cancer with a novel dual targeted conditionally replicative adenovirus (CRAd). Gynecol Oncol 2007;105:113–21, doi:10.1016/j.ygyno.2006.10.057.

44. Diouri M, Keyvani-Amineh H, Geoghegan KF, et al. Cleavage efficiency by adenovirus protease is site-dependent. J Biol Chem 1996;271:32511–4, doi:10.1074/jbc.271.51.32511.

45. Weissleder R, Ntziachristos V. Shedding light onto live molecular targets. Nat Med 2003;9:123–8, doi:10.1038/nm0103-123.

46. Davis SC, Samkoe KS, Tichauer KM, et al. Dynamic dual-tracer MRI-guided fluorescence tomography to quantify receptor density in vivo. Proc Natl Acad Sci U S A 2013;110:9025–30, doi:10.1073/pnas.1213490110.

47. Ntziachristos V, Schellenberger EA, Ripoll J, et al. Visualization of antitumor treatment by means of fluorescence molecular tomography with an annexin V-Cy5.5 conjugate. Proc Natl Acad Sci U S A 2004;101:12294–9, doi:10.1073/pnas.0401137101.

48. Mittal SK, McDermott MR, Johnson DC, et al. Monitoring foreign gene expression by a human adenovirus-based vector using the firefly luciferase gene as a reporter. Virus Res 1993;28:67–90, doi:10.1016/0168-1702(93)90090-A.

49. Tjuvajev JG, Avril N, Oku T, et al. Imaging herpes virus thymidine kinase gene transfer and expression by positron emission tomography. Cancer Res 1998;58:4333–41.

50. Matthews QL, Sibley DA, Wu H, et al. Genetic incorporation of a herpes simplex virus type 1 thymidine kinase and firefly luciferase fusion into the adenovirus protein IX for functional display on the virion. Mol Imaging 2006;5:510–9.

51. Gambhir SS, Barrio JR, Phelps ME, et al. Imaging adenoviral-directed reporter gene expression in living animals with positron emission tomography. Proc Natl Acad Sci U S A 1999;96:2333–8, doi:10.1073/pnas.96.5.2333.

52. Green LA, Nguyen K, Berenji B, et al. A tracer kinetic model for 18F-FHBG for quantitating herpes simplex virus type 1 thymidine kinase reporter gene expression in living animals using PET. J Nucl Med 2004;45:1560–70.

53. Liang Q, Nguyen K, Satyamurthy N, et al. Monitoring adenoviral DNA delivery, using a mutant herpes simplex virus type 1 thymidine kinase gene as a PET reporter gene. Gene Ther 2002;9:1659–66, doi:10.1038/sj.gt.3301899.

54. Pouliot F, Karanikolas BD, Johnson M, et al. In vivo imaging of intraprostatic-specific gene transcription by PET. J Nucl Med 2011;52:784–91, doi:10.2967/jnumed.110.084582.

55. Fontanellas A, Hervas-Stubbs S, Sampedro A, et al. PET imaging of thymidine kinase gene expression in the liver of non-human primates following systemic delivery of an adenoviral vector. Gene Ther 2009;16:136–41, doi:10.1038/gt.2008.122.

56. Penuelas I, Mazzolini G, Boan JF, et al. Positron emission tomography imaging of adenoviral-mediated transgene expression in liver cancer patients. Gastroenterology 2005;128:1787–95, doi:10.1053/j.gastro.2005.03.024.

57. Abate-Daga D, Andreu N, Camacho-Sanchez J, et al. Oncolytic adenoviruses armed with thymidine kinase can be traced by PET imaging and show potent antitumoural effects by ganciclovir dosing. PLoS One 2011;6:e26142, doi:10.1371/journal.pone.0026142.

58. Freytag SO, Barton KN, Brown SL, et al. Replication-competent adenovirus-mediated suicide gene therapy with radiation in a preclinical model of pancreatic cancer. Mol Ther 2007;15:1600–6, doi:10.1038/sj.mt.6300212.

59. Penheiter AR, Russell SJ, Carlson SK. The sodium iodide symporter (NIS) as an imaging reporter for gene, viral, and cell-based therapies. Curr Gene Ther 2012;12:33–47, doi:10.2174/156652312799789235.

60. Barton KN, Tyson D, Stricker H, et al. GENIS: gene expression of sodium iodide symporter for noninvasive imaging of gene therapy vectors and quantification of gene expression in vivo. Mol Ther 2003;8:508–18, doi:10.1016/S1525-0016(03)00153-9.

61. Grunwald GK, Vetter A, Klutz K, et al. Systemic image-guided liver cancer radiovirotherapy using dendrimer-coated adenovirus encoding the sodium iodide symporter as theranostic gene. J Nucl Med 2013;54:1450–7, doi:10.2967/jnumed.112.115493.

62. Merron A, Baril P, Martin-Duque P, et al. Assessment of the Na/I symporter as a reporter gene to visualize oncolytic adenovirus propagation in peritoneal tumours. Eur J Nucl Med Mol Imaging 2010;37:1377–85, doi:10.1007/s00259-009-1379-3.

63. Merron A, Peerlinck I, Martin-Duque P, et al. SPECT/CT imaging of oncolytic adenovirus propagation in tumours in vivo using the Na/I symporter as a reporter gene. Gene Ther 2007;14:1731–8, doi:10.1038/sj.gt.3303043.

64. Oneal MJ, Trujillo MA, Davydova J, et al. Characterization of infectivity-enhanced conditionally replicating adenovectors for prostate cancer radiovirotherapy. Hum Gene Ther 2012;23:951–9, doi:10.1089/hum.2012.047.

65. Peerlinck I, Merron A, Baril P, et al. Targeted radionuclide therapy using a Wnt-targeted replicating adenovirus encoding the Na/I symporter. Clin Cancer Res 2009;15:6595–601, doi:10.1158/1078-0432.CCR-09-0262.

66. Rajecki M, Sarparanta M, Hakkarainen T, et al. SPECT/CT imaging of hNIS-expression after intravenous delivery of an oncolytic adenovirus and 131I. PLoS One 2012;7:e32871, doi:10.1371/journal.pone.0032871.

67. Trujillo MA, Oneal MJ, McDonough S, et al. A probasin promoter, conditionally replicating adenovirus that expresses the sodium iodide symporter (NIS) for radiovirotherapy of prostate cancer. Gene Ther 2010;17:1325–32, doi:10.1038/gt.2010.63.

68. Barton KN, Stricker H, Brown SL, et al. Phase I study of noninvasive imaging of adenovirus-mediated gene expression in the human prostate. Mol Ther 2008;16:1761–9, doi:10.1038/mt.2008.172.

69. Buchsbaum DJ, Chaudhuri TR, Yamamoto M, et al. Gene expression imaging with radiolabeled peptides. Ann Nucl Med 2004;18:275–83, doi:10.1007/BF02984464.

70. Chen R, Parry JJ, Akers WJ, et al. Multimodality imaging of gene transfer with a receptor-based reporter gene. J Nucl Med 2010;51:1456–63, doi:10.2967/jnumed.109.063586.

71. Hemminki A, Zinn KR, Liu B, et al. In vivo molecular chemotherapy and noninvasive imaging with an infectivity-enhanced adenovirus. J Natl Cancer Inst 2002;94:741–9, doi:10.1093/jnci/94.10.741.

72. Rogers BE, Parry JJ, Andrews R, et al. MicroPET imaging of gene transfer with a somatostatin receptor-based reporter gene and (94m)Tc-Demotate 1. J Nucl Med 2005;46:1889–97.

73. Rogers BE, Zinn KR, Buchsbaum DJ. Gene transfer strategies for improving radiolabeled peptide imaging and therapy. Q J Nucl Med 2000;44:208–23.

74. Zinn KR, Chaudhuri TR, Krasnykh VN, et al. Gamma camera dual imaging with a somatostatin receptor and thymidine kinase after gene transfer with a bicistronic adenovirus in mice. Radiology 2002;223:417–25, doi:10.1148/radiol.2232010501.

75. Jacobs A, Tjuvajev JG, Dubrovin M, et al. Positron emission tomography-based imaging of transgene expression mediated by replication-conditional, oncolytic herpes simplex virus type 1 mutant vectors in vivo. Cancer Res 2001;61:2983–95.

76. Goel A, Carlson SK, Classic KL, et al. Radioiodide imaging and radiovirotherapy of multiple myeloma using VSV(Delta51)-NIS, an attenuated vesicular stomatitis virus encoding the sodium iodide symporter gene. Blood 2007;110:2342–50, doi:10.1182/blood-2007-01-065573.

77. Gholami S, Chen CH, Belin LJ, et al. Vaccinia virus GLV-1h153 is a novel agent for detection and effective local control of positive surgical margins for breast cancer. Breast Cancer Res 2013;15:R26, doi:10.1186/bcr3404.

78. Gholami S, Haddad D, Chen CH, et al. Novel therapy for anaplastic thyroid carcinoma cells using an oncolytic vaccinia virus carrying the human sodium iodide symporter. Surgery 2011; 150:1040–7, doi:10.1016/j.surg.2011.09.010.

79. Haddad D, Chen CH, Carlin S, et al. Imaging characteristics, tissue distribution, and spread of a novel oncolytic vaccinia virus carrying the human sodium iodide symporter. PLoS One 2012;7: e41647, doi:10.1371/journal.pone.0041647.

80. Haddad D, Chen NG, Zhang Q, et al. Insertion of the human sodium iodide symporter to facilitate deep tissue imaging does not alter oncolytic or replication capability of a novel vaccinia virus. J Transl Med 2011;9:36, doi:10.1186/1479-5876-9-36.

81. Haddad D, Zanzonico PB, Carlin S, et al. A vaccinia virus encoding the human sodium iodide symporter facilitates long-term image monitoring of virotherapy and targeted radiotherapy of pancreatic cancer. J Nucl Med 2012;53:1933–42, doi:10.2967/jnumed.112.105056.

82. Carlson SK, Classic KL, Hadac EM, et al. Quantitative molecular imaging of viral therapy for pancreatic cancer using an engineered measles virus expressing the sodium-iodide symporter reporter gene. AJR Am J Roentgenol 2009;192:279–87, doi:10.2214/AJR.08.1205.

83. Dingli D, Peng KW, Harvey ME, et al. Image-guided radio-virotherapy for multiple myeloma using a recombinant measles virus expressing the thyroidal sodium iodide symporter. Blood 2004;103:1641–6, doi:10.1182/blood-2003-07-2233.

84. Hasegawa K, Pham L, O'Connor MK, et al. Dual therapy of ovarian cancer using measles viruses expressing carcinoembryonic antigen and sodium iodide symporter. Clin Cancer Res 2006;12: 1868–75, doi:10.1158/1078-0432.CCR-05-1803.

85. Msaouel P, Dispenzieri A, Galanis E. Clinical testing of engineered oncolytic measles virus strains in the treatment of cancer: an overview. Curr Opin Mol Ther 2009;11:43–53.

86. Msaouel P, Iankov ID, Allen C, et al. Noninvasive imaging and radiovirotherapy of prostate cancer using an oncolytic measles virus expressing the sodium iodide symporter. Mol Ther 2009;17: 2041–8, doi:10.1038/mt.2009.218.

87. Penheiter AR, Dingli D, Bender CE, et al. Monitoring the initial delivery of an oncolytic measles virus encoding the human sodium iodide symporter to solid tumors using contrast-enhanced computed tomography. J Gene Med 2012;14:590–7, doi:10.1002/jgm.2670.

88. McCart JA, Mehta N, Scollard D, et al. Oncolytic vaccinia virus expressing the human somatostatin receptor SSTR2: molecular imaging after systemic delivery using 111In-pentetreotide. Mol Ther 2004;10:553–61, doi:10.1016/j.ymthe.2004.06.158.

89. Rogers BE, Zinn KR, Lin CY, et al. Targeted radiotherapy with [(90)Y]-SMT 487 in mice bearing human nonsmall cell lung tumor xenografts induced to express human somatostatin receptor subtype 2 with an adenoviral vector. Cancer 2002;94:1298–305, doi:10.1002/cncr.10300.

90. Yang D, Han L, Kundra V. Exogenous gene expression in tumors: noninvasive quantification with functional and anatomic imaging in a mouse model. Radiology 2005;235:950–8, doi:10.1148/radiol.2353040108.

91. Lohr F, Huang Q, Hu K, et al. Systemic vector leakage and transgene expression by intratumorally injected recombinant adenovirus vectors. Clin Cancer Res 2001;7:3625–8.

92. Wang Y, Hu JK, Krol A, et al. Systemic dissemination of viral vectors during intratumoral injection. Mol Cancer Ther 2003;2: 1233–42.

93. Wang Y, Yang Z, Liu S, et al. Characterisation of systemic dissemination of nonreplicating adenoviral vectors from tumours in local gene delivery. Br J Cancer 2005;92:1414–20, doi:10.1038/sj.bjc.6602494.

94. Trujillo MA, Oneal MJ, McDonough SJ, et al. Viral dose, radioiodide uptake, and delayed efflux in adenovirus-mediated NIS radiovirotherapy correlates with treatment efficacy. Gene Ther 2013;20:567–74, doi:10.1038/gt.2012.71.

95. Siddiqui F, Barton KN, Stricker HJ, et al. Design considerations for incorporating sodium iodide symporter reporter gene imaging into prostate cancer gene therapy trials. Hum Gene Ther 2007;18: 312–22, doi:10.1089/hum.2006.131.

96. Hakkarainen T, Rajecki M, Sarparanta M, et al. Targeted radiotherapy for prostate cancer with an oncolytic adenovirus coding for human sodium iodide symporter. Clin Cancer Res 2009;15:5396–403, doi:10.1158/1078-0432.CCR-08-2571.

97. Barton KN, Stricker H, Elshaikh MA, et al. Feasibility of adenovirus-mediated hNIS gene transfer and 131I radioiodine therapy as a definitive treatment for localized prostate cancer. Mol Ther 2011;19:1353–9, doi:10.1038/mt.2011.89.

98. Massoud TF, Gambhir SS. Molecular imaging in living subjects: seeing fundamental biological processes in a new light. Genes Dev 2003;17:545–80, doi:10.1101/gad.1047403.

99. Kim YJ, Dubey P, Ray P, et al. Multimodality imaging of lymphocytic migration using lentiviral-based transduction of a tri-fusion reporter gene. Mol Imaging Biol 2004;6:331–40, doi:10.1016/j.mibio.2004.06.009.

100. Ray P, De A, Min JJ, et al. Imaging tri-fusion multimodality reporter gene expression in living subjects. Cancer Res 2004;64: 1323–30, doi:10.1158/0008-5472.CAN-03-1816.
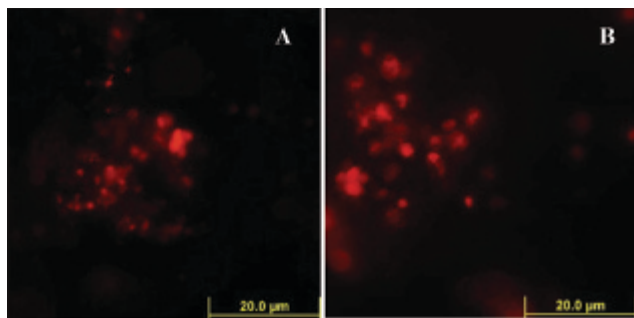
Figure S1. Representative images of mCherry-positive cells visualized using fluorescence microscopy in the tumor tissue extracted from mice 6 days after injection of Ad5/3Δ24pIXcherry/SSTR (A) or control Ad5/3Δ24pIXcherry (B). The images of fluorescent cells are shown at a magnification of 100×. The scale bar represents 20 μm.